1051-H-11
Y3.N88:25/4583/v3
SEP 25 1987

NUREG/CR-4583
PNL-5822
Vol. 3

Development and Validation of a Real-Time SAFT-UT System for the Inspection of Light Water Reactor Components

Annual Report
October 1985 - September 1986

Prepared by S. R. Doctor, T. E. Hall, L. D. Reid, G. A. Mart

Pacific Northwest Laboratory
Operated by
Battelle Memorial Institute

Prepared for
U.S. Nuclear Regulatory Commission

ORIGINAL

COMPLETED

Y4/C53

NOTICE

This report was prepared as an account of work sponsored by an agency of the United States Government. Neither the United States Government nor any agency thereof, or any of their employees, makes any warranty, expressed or implied, or assumes any legal liability of responsibility for any third party's use, or the results of such use of any information, apparatus, product or process disclosed in this report, or represents that its use by such third party would not infringe privately owned rights.

NOTICE

Availability of Reference Materials Cited in NRC Publications

Most documents cited in NRC publications will be available from one of the following sources:

1. The NRC Public Document Room, 1717 H Street, N.W.
   Washington, DC 20555
2. The Superintendent of Documents, U.S. Government Printing Office, Post Office Box 37082,
   Washington, DC 20013-7082
3. The National Technical Information Service, Springfield, VA 22161

Although the listing that follows represents the majority of documents cited in NRC publications, it is not intended to be exhaustive.

Referenced documents available for inspection and copying for a fee from the NRC Public Document Room include NRC correspondence and internal NRC memoranda; NRC Office of Inspection and Enforcement bulletins, circulars, information notices, inspection and investigation notices; Licensee Event Reports; vendor reports and correspondence; Commission papers; and applicant and licensee documents and correspondence.

The following documents in the NUREG series are available for purchase from the GPO Sales Program: formal NRC staff and contractor reports, NRC-sponsored conference proceedings, and NRC booklets and brochures. Also available are Regulatory Guides, NRC regulations in the *Code of Federal Regulations*, and *Nuclear Regulatory Commission Issuances*.

Documents available from the National Technical Information Service include NUREG series reports and technical reports prepared by other federal agencies and reports prepared by the Atomic Energy Commission, forerunner agency to the Nuclear Regulatory Commission.

Documents available from public and special technical libraries include all open literature items, such as books, journal and periodical articles, and transactions. *Federal Register* notices, federal and state legislation, and congressional reports can usually be obtained from these libraries.

Documents such as theses, dissertations, foreign reports and translations, and non-NRC conference proceedings are available for purchase from the organization sponsoring the publication cited.

Single copies of NRC draft reports are available free, to the extent of supply, upon written request to the Division of Information Support Services, Distribution Section, U.S. Nuclear Regulatory Commission, Washington, DC 20555.

Copies of industry codes and standards used in a substantive manner in the NRC regulatory process are maintained at the NRC Library, 7920 Norfolk Avenue, Bethesda, Maryland, and are available there for reference use by the public. Codes and standards are usually copyrighted and may be purchased from the originating organization or, if they are American National Standards, from the American National Standards Institute, 1430 Broadway, New York, NY 10018.

NUREG/CR-4583
PNL-5822
Vol. 3
R5

Development and Validation of a Real-Time SAFT-UT System for the Inspection of Light Water Reactor Components

Annual Report
October 1985 - September 1986

Manuscript Completed: May 1987
Date Published: July 1987

Prepared by
S. R. Doctor, T. E. Hall, L. D. Reid, G. A. Mart

Pacific Northwest Laboratory
Richland, WA 99352

Prepared for
Division of Engineering
Office of Nuclear Regulatory Research
U.S. Nuclear Regulatory Commission
Washington, DC 20555
NRC FIN B2467

PREVIOUS REPORTS AND SERIES

L. J. Busse, H. D. Collins, and S. R. Doctor. 1984. Review and Discussion of the Development of Synthetic Aperture Focusing Technique for Ultrasonic Testing (SAFT-UT). NUREG/CR-3625, PNL-4957. Pacific Northwest Laboratory, Richland, Washington.

S. R. Doctor, L. J. Busse, S. L. Crawford, T. E. Hall, R. P. Gribble, A. J. Baldwin, and L. P. Van Houten. 1986. Development and Validation of a Real-Time SAFT-UT System for the Inspection of Light Water Reactor Components. NUREG/CR-4583, PNL-5822, Vol. 1. Pacific Northwest Laboratory, Richland, Washington.

S. R. Doctor and T. E. Hall. 1987. Development and Validation of a Real-Time SAFT-UT System for the Inspection of Light Water Reactor Components. NUREG/CR-4583, PNL-5822, Vol. 2. Pacific Northwest Laboratory, Richland, Washington.

ABSTRACT

The Pacific Northwest Laboratory is working to design, fabricate, and evaluate a real-time flaw detection and characterization system based on the synthetic aperture focusing technique for ultrasonic testing (SAFT-UT). The system is designed to perform inservice inspection of light-water reactor components. Included objectives of this program for the Nuclear Regulatory Commission are to develop procedures for system calibration and field operation, to validate the system through laboratory and field inspections, and to generate an engineering data base to support ASME Code acceptance of the technology. This progress report covers the programmatic work from October 1985 through September 1986.

iv

EXECUTIVE SUMMARY

A multi-year program for the Development and Validation of a Real-Time SAFT-UT System for Inservice Inspection of Light Water Reactors was established at the Pacific Northwest Laboratory (PNL) to develop the synthetic aperture focusing technique (SAFT) and demonstrate the technology in reactor inservice inspections.

The objectives of this program for the Nuclear Regulatory Commission (NRC) include these:

- Design, fabricate, and evaluate a real-time flaw detection and characterization system based on SAFT-UT for inservice inspection (ISI) of all required LWR components.
- Establish calibration and field operating procedures.
- Demonstrate and validate the SAFT-UT system through actual reactor inservice inspections.
- Generate an engineering data base to support ASME Code acceptance of the real-time SAFT-UT technology.

The scope of the program is defined by the following:

- Conduct laboratory tests to provide engineering data for defining SAFT-UT system performance.
- Complete the development of a special processor to make SAFT a real-time process for ISI applications.
- Fabricate and field test a real-time SAFT-UT system suitable for field inspection of nuclear reactor piping, nozzles, and pressure vessels.

During this year, a formal agreement was put in place with Combustion Engineering in which they joined the program and began assisting in validating the SAFT technology on nuclear power plants.

On-going work is focused on advancing the evolution of the SAFT field system from concept to reality. The final field system was operational by the end of the fiscal year 1985; and the emphasis this past year has been in terms of parametric sensitivity studies on operational parameters, further development of the real-time SAFT processor box, and detailed analysis of a number of defected samples.

The tandem SAFT mode was developed in 1985 to overcome some of the serious shortcomings of the pulse-echo mode. This first implementation of the TSAFT mode was developed by using a fixed source and scanned receiver. During this year, the TSAFT-2 mode was developed, which uses a scanned source and scanned receiver. The performance of the TSAFT-2 mode is clearly superior and allows defects with depth larger than the transducer beam diameter to be sized accurately and shows an improvement of the resolution performance.

Extensive efforts were expended to conduct parametric studies on the sensitivity of the SAFT system to some of the processing variables. The variables studied during this reporting period included: pulse-echo sampling rate, 3-D SAFT mode versus the Line-SAFT mode, TSAFT velocity changes of up to ±20%, TSAFT thickness changes of up to ±20%, TSAFT resolution performance, imaging of non-vertical defects, and performance of TSAFT and TSAFT-2 for accurately sizing vertical defects. The SAFT system performed as predicted based on theory. As the sampling rate increased, the imaging resolution improved until twice the Nyquist sampling rate was achieved. The resolution performance of the 3-D SAFT mode was shown to be very superior to the results for Line-SAFT for reflectors exhibiting high spatial frequencies. The surprising result for changes in velocity and thickness was to have a large shift in the defect location and a minor blurring or resolution loss in the image. The SAFT system performance deteriorated the same as other acoustic methods because of signal loss when defects became non-vertical and scattered the acoustic energy outside the receiver aperture. The changes are documented and predictable from simple acoustic scattering theory. The superiority of the TSAFT-2 mode over the original TSAFT configuration was demonstrated through a series of sawcut sizing measurements showing the increase in resolution performance by a factor of 1.4.

The evolution of the real-time SAFT processor box is continuing, and further studies of the performance is showing that the real-time rates of ten A-scans per second can be achieved when the new 68020 microprocessor boards are used.

Some very good studies were performed in the laboratory on blocks and pipe specimens from a number of sources. The SAFT performance was very good and was within predictions for the apertures that the specimens allowed. TSAFT-2 was shown to provide improved near-surface performance over pulse-echo on the NAVSEA block. The large-diameter pipes in the Materials Reliability Center at PNL were examined and much was learned about refining the SAFT procedure to minimize efforts during the data collection phase. Furthermore, it was found that if the electronics saturate, the resultant image will be blurred and result in systematic oversizing of the defect. Data were collected on a series of KAPL specimens, and the images were good although no feedback has been received on the SAFT result versus the destructive results or even intended defects. Results were obtained on a series of CCSS specimens and all thermal fatigue cracks in the specimens were detected; but at the same time, a number of false calls were made. The false calls result from the coherent backscattering that is produced by the large anisotropic grain structure. Data were also collected on a series of 45 quadrants of pipe specimens that are part of the Mini-Round Robin study in progress at PNL. These data were analyzed and has not been compared with true-state destructive results. This is planned for next fiscal year.

CONTENTS

		Page	
Abstract		iii	
Executive Summary		v	
1.0	Introduction	1-1	1
2.0	Alternate SAFT-UT Tandem Configuration Development (TSAFT-2)	2-1	3
3.0	SAFT-UT Parameter Sensitivity Analysis	3-1	8
3.1	SAFT-UT Pulse-Echo Sampling Study	3-1	8
3.2	SAFT-UT Pulse-Echo Full 3-D SAFT Benefit Study	3-4	11
3.3	TSAFT Velocity and Thickness Variation Study	3-7	14
3.4	SAFT-UT Imaging of Non-Vertical Defects	3-10	17
3.5	TSAFT and TSAFT-2 Sizing Performance on Machined Vertical Sawcuts	3-20	27
4.0	Real-Time SAFT Processor Development	4-1	30
5.0	SAFT-UT Data Collection and Analysis	5-1	32
5.1	NAVSEA Block Data Collection and Analysis	5-1	32
5.2	Materials Reliability Center (MRC) Test Stands	5-9	40
5.2.1	SAFT-UT Data Collection Procedure on Piping Components	5-16	47
5.2.2	SAFT-UT Image Analysis Procedure on Piping Components	5-17	48
5.3	SAFT-UT Data Collection and Analysis on KAPL Specimens	5-18	49
5.4	CCSS Data Collection and Analysis	5-20	50
5.5	Mini-Round Robin (MRR) IGSCC Samples	5-20	50
6.0	Conclusions	6-1	52
7.0	Future Plans	7-1	53
8.0	Bibliography	8-1	54

FIGURES

		Page	
2.1	Shear-Wave Beam Profile of Ideal Point Illuminator in Steel . .	2-1	3
2.2	TSAFT Central Ray Paths for Illumination of Two Object Points Located on a Vertical Plane	2-2	4
2.3	TSAFT Image of Opposing Vertical Sawcuts in 1.0-inch Aluminum (5.0 MHz)	2-3	5
2.4	TSAFT-2 Central Ray Paths for Illumination of Two Object Points Located on a Single Vertical Plane	2-3	5
2.5	TSAFT-2 Image of Opposing Vertical Sawcuts in 1.0-inch Aluminum (5.0 MHz)	2-4	6
2.6	TSAFT-2 Image of Defect in NAVSEA Submarine Sample (5.0 MHz)	2-5	7
3.1	Resolution Analysis Block	3-2	9
3.2	T-VIEW Projection of SAFT-UT Reconstruction of "Y" Pattern	3-3	10
3.3	T-VIEW Projection of SAFT-UT Reconstruction of "Y" Pattern	3-3	10
3.4	T-VIEW Projection of SAFT-UT Reconstruction of "Y" Pattern	3-4	11
3.5	"Parent" Unprocessed "Y" Pattern Data File	3-5	12
3.6	Full 3-D SAFT Reconstruction of the "Y" Pattern Data File	3-6	13
3.7	LINE-SAFT Reconstruction of "Y" Pattern Data File	3-6	13
3.8	LINE-SAFT Reconstruction Subsequent to Envelope Detection of the "Y" Pattern Data File	3-7	14
3.9	TSAFT Velocity Sensitivity Study Sequence	3-9	16
3.10	TSAFT Thickness Parameter Sensitivity Study Sequence	3-11	18
3.11	SAFT-UT Pulse-Echo Image of Vertical Sawcut	3-12	19
3.12	SAFT-UT Pulse-Echo Image of a +35° Slanted Sawcut	3-13	20
3.13	SAFT-UT Pulse-Echo Image of a -35° Slanted Sawcut	3-13	20

		Page	
3.14	SAFT-UT Pulse-Echo Configuration Peak Signal Response vs. Machined Defect Slant Angle	3-14	21
3.15	SAFT-UT Tandem Configuration Peak Signal Response vs. Machined Defect Slant Angle	3-15	22
3.16	TSAFT and TSAFT-2 Configuration Image Maximum Value vs. Machined Defect Slant Angle	3-15	22
3.17	TSAFT Image of +10° Slanted Sawcut	3-16	23
3.18	TSAFT-2 Image of +10° Slanted Sawcut	3-17	24
3.19	TSAFT Image of +20° Slanted Sawcut	3-18	25
3.20	TSAFT-2 Image of +20° Slanted Sawcut	3-18	25
3.21	TSAFT Vertical Prediction vs. Machined Defect Slant Angle	3-19	26
3.22	TSAFT-2 Vertical Position vs. Machined Defect Slant Angle	3-20	27
3.23	TSAFT Vertical Prediction vs. Machined Defect Size	3-21	28
3.24	TSAFT-2 Vertical Prediction vs. Machined Defect Size	3-21	28
5.1	Dimensions and Reference Lines of PISC II Block Number 2	5-2	33
5.2	Pulse-Echo Image from the Top of the Plate at 2.25 MHz and 45° showing Defect Number 1	5-4	35
5.3	Pulse-Echo Image from the Top of the Plate at 5 MHz and 45° showing Defect Number 1	5-4	36
5.4	Pulse-Echo Image from the Top of the Plate at 2.25 MHz and 60° showing Defect Number 1 and Number 2	5-5	37
5.5	TSAFT Image from the Top of the Plate at 2.25 MHz and 45° showing Defect Number 1	5-6	38
5.6	TSAFT Image from the Top of the Plate at 5 MHz and 45° showing Defect Number 1	5-6	38
5.7	TSAFT-2 Image from the Top of the Plate at 5 MHz showing Defect Number 1 and Number 3	5-6	38
5.8	Pulse-Echo Image from the Bottom of the Plate at 2.25 MHz showing Defect Number 1 and Number 3	5-8	39
5.9	TSAFT Image from the Bottom of the Plate at 2.25 MHz of Defect Number 3	5-8	39

		Page	
5.10	Test Specimen Configuration	5-10	41
5.11	Photograph of Inside Diameter of N4/N5 at 71.5-inch Location	5-14	45
5.12	SAFT-UT Pulse-Echo Image of Notch and Cracking in N4 Region from 74.0 to 70.25 Inches	5-15	46
5.13	TSAFT-2 Image of Notch and Cracking in N4 Region from 74.0 to 70.25 Inches	5-15	46
5.14	Transducer Beam Profile through Cladding Material	5-19	50
5.15	Transducer Beam Profile through Cladding Material	5-19	50

TABLES

		Page	
3.1	Flow Diagram of Three SAFT-UT Processing Options	3-5	12
4.1	Estimated Real-Time SAFT Processor Performance (-20 dB Selective Processing Implemented)	4-2	31
4.2	Estimated Real-Time SAFT Processor Performance (No Selective Processing Implemented)	4-2	31
5.1	SAFT-UT Inspection Configurations Performed on NAVSEA Test Plate	5-3	34
5.2	Size and Nature of Three Detected Defects in NAVSEA Plate . . .	5-7	38
5.3	Actual Crack Depths from Core Samples	5-11	42
5.4	Comparison of SAFT-UT Vertical Sizing Performance and Actual Measured Crack Depth	5-12	43
5.5	Transducer Profile Color Scale	5-20	51

DEVELOPMENT OF A REAL-TIME SAFT-UT SYSTEM FOR THE INSPECTION OF LIGHT WATER REACTOR COMPONENTS

1.0 INTRODUCTION

The basic functions of all nondestructive testing (NDT) procedures in the nuclear power industry are: 1) to detect flaws or defects within structural and functional components; and 2) to classify and/or characterize the detected defects by their size, shape, orientation, location, and composition (cracks, voids, inclusions, etc.) so that rational decisions about reactor safety can be made. Synthetic Aperture Focusing Technique for Ultrasonic Testing (SAFT-UT) is an imaging technique designed to enhance conventional ultrasonic NDT procedures for performing these two basic functions.

SAFT-UT is a particularly flexible imaging method that can be adapted to many different types of materials, specimen geometries, and ultrasonic propagation modes. This flexibility makes SAFT-UT imaging well suited to industrial applications. The spatial averaging inherent in SAFT-UT processing can be used to enhance the signal-to-noise ratio present in all conventional ultrasonic tests. Improved signal-to-noise ratios facilitate the detection of small defects. SAFT-UT processing can provide high-resolution images of detected defects. The images produced are volumetric; i.e., they are a three-dimensional map of the defect and surrounding region. Such a map, when accurately interpreted, can aid decisions about the integrity of critical components that affect the safety and reliability of reactor operation.

In 1974 the U.S. Nuclear Regulatory Commission (NRC) initiated a program at the University of Michigan to develop SAFT for nuclear applications. This program continued through 1982 at the University of Michigan in the "laboratory" phase. In 1982, a multi-year program was started at the Pacific Northwest Laboratory (PNL) for the "field-application" phase. The objectives of the PNL effort are:

- Provide the engineering required to design and develop a real-time SAFT-UT imaging system for the inservice inspection of light-water reactor system components.
- Evaluate the SAFT-UT field system.
- Develop the engineering data base to establish Code and regulatory acceptance of SAFT imaging procedures.

This report covers the third year of activities.

The several sections of this report discuss different parts of SAFT-UT development:

- Section 2 provides the technical details of the development of the TSAFT-2 mode of operation.

0001

- Section 3 gives the results of parametric sensitivity studies for pulse-echo samples, 3-D mode versus Line-SAFT, TSAFT velocity, TSAFT thickness, TSAFT resolution, imaging of non-vertical defects, and TSAFT and TSAFT-2 sizing performance on vertical defects.

- Section 4 describes the progress on the real-time processor in terms of the hardware and software developments.

- Section 5 describes the engineering data bases that were used in the evaluation of the SAFT technology.

- Section 6 provides conclusions generated from this year's work effort.

- Section 7 provides the direction for work to be conducted in fiscal year 1987.

0002

2.0 ALTERNATE SAFT-UT TANDEM CONFIGURATION DEVELOPMENT (TSAFT-2)

SAFT-UT scan configurations incorporate a point illuminator, thus generating a divergent sound field in the object of interest; and, typically, shear-wave angle-beam techniques are utilized in the inspection of light-water reactor components. The original TSAFT configuration implements a fixed transmitter and scanned receiver illumination scheme. During an experimental effort to evaluate the resolution performance of this technique, it was noted that the TSAFT configuration introduces a limitation with respect to illumination of large vertical defects. A degradation of the resulting image was observed due to an aperture-limiting effect of the fixed transmitter.

Shear-mode configurations inherently exhibit a phenomenon that occurs at the transducer-to-steel interface, which shapes the illumination intensity. It can be shown that the transmission coefficient at the material interface is a function of angle (Krautkramer and Krautkramer, 1977), with the resulting beam pattern, for an ideal point illuminator and receiver, altered to that which is shown in Figure 2.1. One can see immediately that, since the transmitter is fixed in the TSAFT mode, a high illumination intensity will occur where the 38° ray intersects the object plane. In fact, the lower angles (less than 33°) will be significantly attenuated.

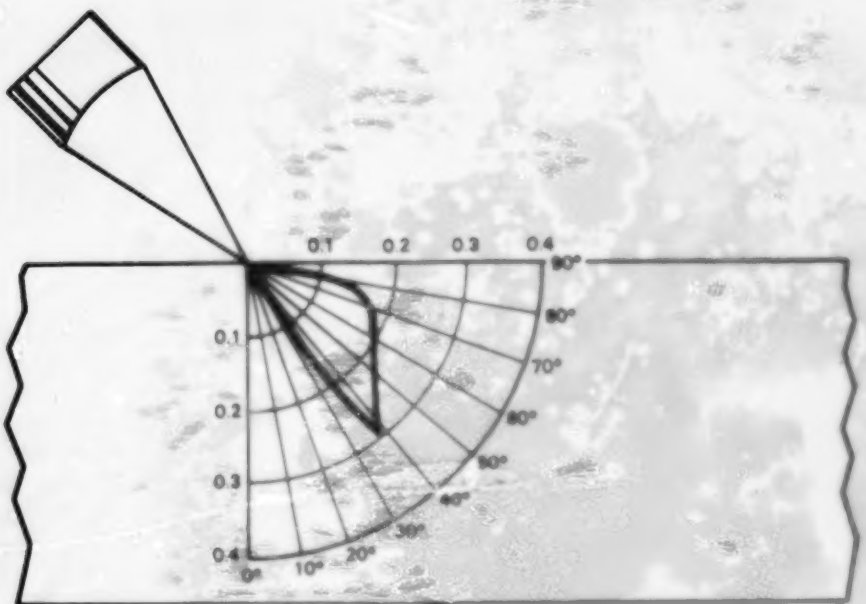

FIGURE 2.1. Shear-Wave Beam Profile of Ideal Point Illuminator in Steel

0003

BEST COPY AVAILABLE

Figure 2.2 shows a diagram of typical TSAFT sound paths in material with a finite thickness. The central rays are shown illuminating two object points (P_1 and P_2) located on a given object plane. It is apparent from this diagram that the angles of illumination (ϕ_1 and ϕ_2) are not equal; and from the previous discussion, it can be stated that the intensities of the two rays will, in general, not be the same. So, even if a wide angle point transmitter is utilized in this configuration, illumination of a vertical object plane in a uniform manner throughout the scanned aperture is not possible.

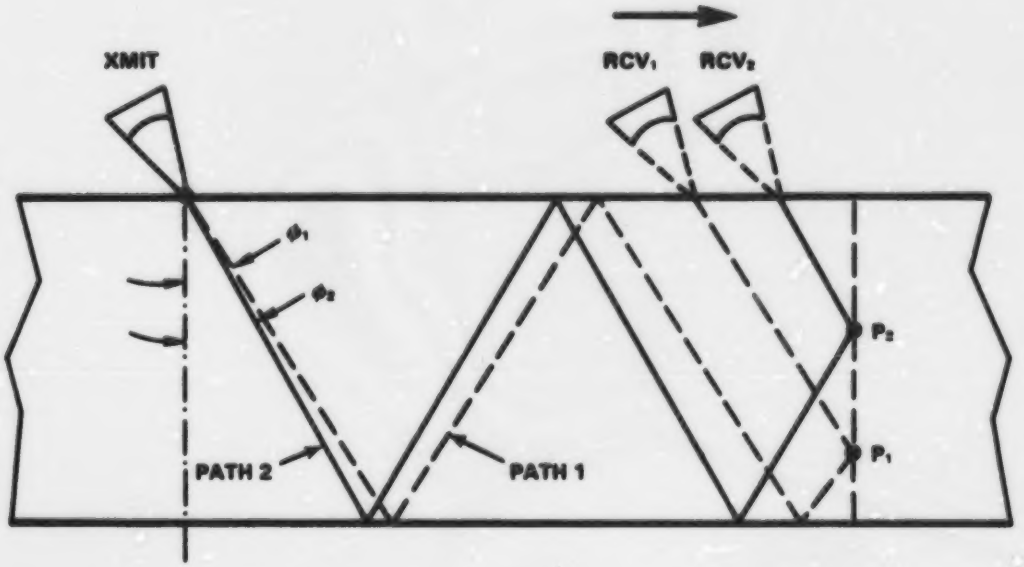

FIGURE 2.2. TSAFT Central Ray Paths for Illumination of Two Object Points Located on a Vertical Plane

Figure 2.3 shows a TSAFT image of a test block with two opposing vertical sawcuts placed in a 1.0-inch-thick aluminum coupon. One was cut from the front surface and the second was cut from the back surface, exactly opposite from the first. Each cut makes a semi-circular shape 3.32-inches long and 0.475 inches into the material; so the separation at the center of the piece is 0.050 inches. It can be noted from this photograph that the TSAFT (Tandem SAFT) configuration, using a fixed transmitter and a scanned receiver, does not illuminate the vertical reflector throughout the full extent of the object. Rather, the illumination distribution in the scan direction is dominated by the material interface response at the entry of the divergent sound beam (Figure 2.1). Using a 5.0-MHz contact transducer with a diameter of 0.25 inches, the illumination extends to approximately 1/2T in the vertical direction. This is with a 3/2-Vee transmitter bounce path and the transmitting probe placed such that the center ray strikes the base of the object plane (i.e., sawcut base and lower surface intersection).

0004

BEST COPY AVAILABLE

FIGURE 2.3. TSAFT Image of Opposing Vertical Sawcuts in 1.0-inch Aluminum (5.0 MHz)

To overcome this, another tandem configuration (TSAFT-2) was developed. This technique simultaneously scans the transmitter in the opposite direction as the receiver, thus maintaining a constant direct illumination angle in any given vertical plane. Figure 2.4 shows the expected central ray paths when implementing the TSAFT-2 configuration. Both transducers are simultaneously

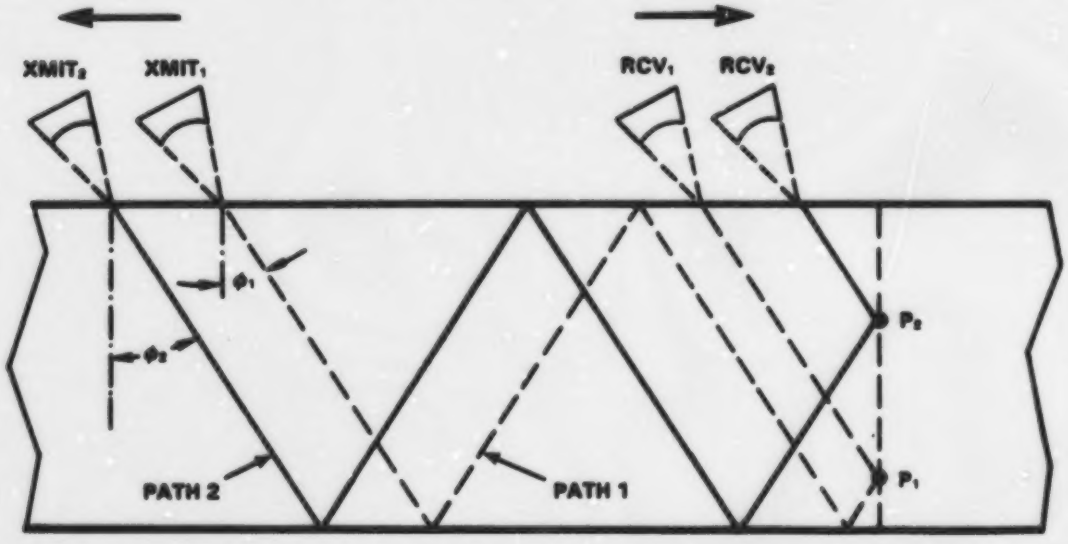

FIGURE 2.4. TSAFT-2 Central Ray Paths for Illumination of Two Object Points Located on a Single Vertical Plane

BEST COPY AVAILABLE

scanned in opposite directions and at the same rate. The object points (P_1 and P_2) for path 1 and path 2 are located in one vertical plane. Note in Figure 2.4 that the illumination angles (ϕ_1 and ϕ_2) are equal. This is the objective of this configuration so that the central angle of illumination is constant throughout a given object plane. When reviewing Figure 2.1, it can then be seen that the TSAFT-2 configuration achieves constant illumination for given vertical planes.

Figure 2.5 shows the TSAFT-2 image of the opposing sawcut coupon previously described for the TSAFT configuration. A dramatic improvement in illumination is realized, and both sawcut reflectors can be clearly seen. Also, it should be noted that near-surface imaging is greatly improved utilizing this technique.

FIGURE 2.5. TSAFT-2 Image of Opposing Vertical Sawcuts in 1.0-inch Aluminum (5.0 MHz)

A submarine hull weld specimen was received in January 1986 and thus provided an opportunity to utilize TSAFT-2 on another test sample. Figure 2.6 shows a 5-MHz TSAFT-2 image of a particular area of interest in this specimen. Two defects can be clearly seen in the B-scan end view presentation, and of specific merit is the near-surface indication. When scanning this area, no other configuration revealed this indication because of its proximity to the front surface. The TSAFT-2 image suggested that there was a near-surface indication; and subsequent scans conducted from the opposite surface verified the presence of this defect.

Incorporation of the TSAFT-2 algorithm in the SAFT-UT utility set has proved to be a valuable asset for sizing vertically oriented and volumetric defects in thin materials. Near-surface imaging is greatly enhanced; and, as

BEST COPY AVAILABLE

FIGURE 2.6. TSAFT-2 Image of Defect in NAVSEA Submarine Sample (5.0 MHz)

will be discussed later, a resolution improvement is realized when compared with the original TSAFT configuration. The software for utilization of the TSAFT-2 algorithm has been completed and is implemented in the SAFT-UT utility set. Further work is planned to fully investigate the imaging capabilities of the TSAFT-2 configuration.

BEST COPY AVAILABLE

3.0 SAFT-UT PARAMETER SENSITIVITY ANALYSIS

A number of parametric studies were performed to evaluate the ideal performance of the various SAFT-UT configurations. This is an on-going effort, with additional analysis planned for next year. This analysis is intended to assist the SAFT-UT operator in optimizing the data collection process and provide the foundation necessary to accurately interpret the resulting images. The studies conducted this year were: SAFT-UT pulse-echo sampling study, SAFT-UT pulse-echo full 3-D benefit study, TSAFT velocity and thickness variation study, SAFT-UT imaging of non-vertical defects, and TSAFT and TSAFT-2 sizing performance on machined vertical sawcuts.

3.1 SAFT-UT PULSE-ECHO SAMPLING STUDY

Analysis was performed in early October 1985 with respect to determining the optimum sampling, both spatially and temporally, required by the SAFT-UT pulse-echo algorithm. A test pattern was placed in aluminum material and is illustrated in Figure 3.1. Seven flat-bottom holes were drilled in a "Y" pattern at a 45° angle from the normal. Each hole is 0.188 inches in diameter. The legs of the "Y" are drilled such that there is a center-to-center spacing of 0.227, 0.268 and 0.348 inches; or for a 2.25-MHz shear-mode inspection, this can be expressed as 4.5, 5.4 and 7 wavelengths, with a separation of 0.039, 0.078, and 0.157 inches or 0.71, 1.42, and 2.85 wavelengths. This pattern provides a sufficiently complex object for this study, with components on the order of a resolution distance apart.

Figure 3.2 shows a photograph of the initial SAFT-UT image of the "Y" pattern object. The T-VIEW feature of the SAFT analysis graphics package has been utilized for this image. This view is of a plane perpendicular to the transducer insonification direction. The lateral optical incremental distance between A-scans was 0.05 inches, or about one wavelength. The temporal sampling was 50 nsec, or eight samples per wavelength. The quality of the image is very good, with the closer spaced holes just being resolved. Using this image as the reference set, further scans were performed at larger increments to observe image degradation.

Figure 3.3 shows an image of the same "Y" pattern, but the temporal sampling was set to 100 nsec, or four samples per wavelength. This was considered as coarse a temporal sampling as is desirable since the Nyquist frequency is being approached. This image is very good and comparable with Figure 3.2.

The lateral sampling was then adjusted to 0.1 inches, or about two wavelengths. This image is shown in Figure 3.4. A degradation in image quality can be easily seen in this presentation.

The conclusion drawn from this study is that a sampling of one wavelength or finer is necessary in the lateral direction. In the temporal direction, a sampling rate of a fourth of the wavelength or finer is necessary. This is in agreement with the results from University of Michigan's parametric studies.

0008

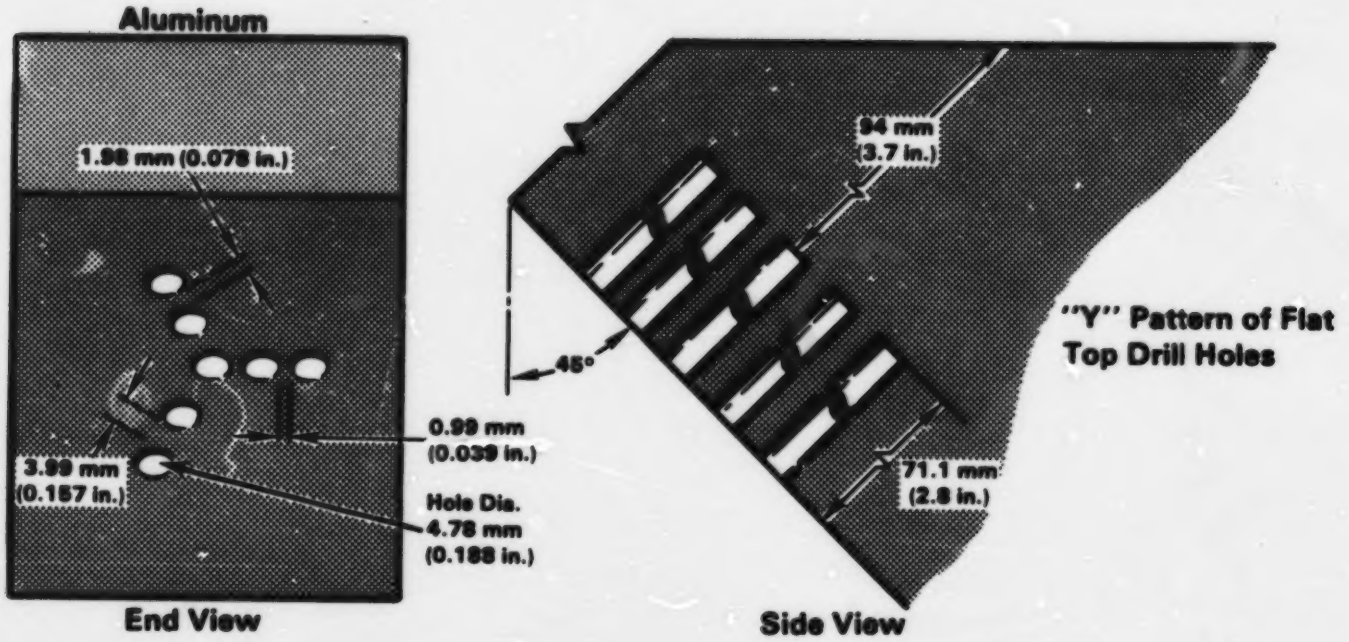

FIGURE 3.1. Resolution Analysis Block

BEST COPY AVAILABLE

FIGURE 3.2. T-VIEW Projection of SAFT-UT Reconstruction of "Y" Pattern (lateral increment = 0.005 inches; temporal sampling = 8 samples/wavelength)

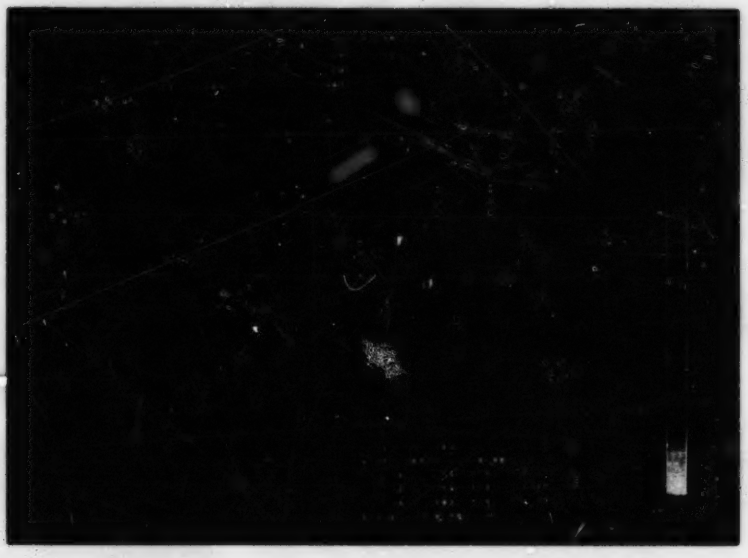

FIGURE 3.3. T-VIEW Projection of SAFT-UT Reconstruction of "Y" Pattern (lateral resolution = 0.05 inches; temporal sampling = 4 samples/wavelength)

BEST COPY AVAILABLE

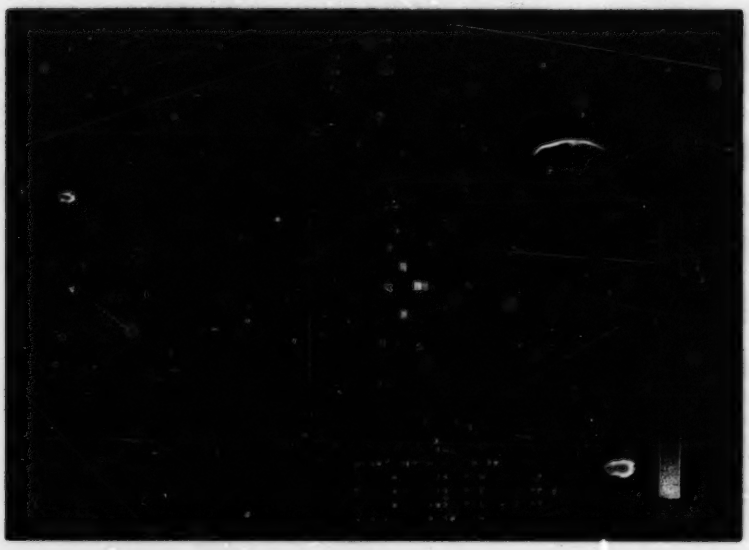

FIGURE 3.4. T-VIEW Projection of SAFT-UT Reconstruction of "Y" Pattern (lateral resolution of 0.1 inch; temporal sampling = 4 samples/ wavelength)

3.2 SAFT-UT PULSE-ECHO FULL 3-D SAFT BENEFIT STUDY

The question of the benefits of performing the full three-dimensional SAFT as compared with other less computationally intensive methods has been debated for some time. Intuitively, if the effect of all dimensions is not computed, or if the temporal phase information is not included, one would expect some image degradation to occur. The real question is how much quality does one sacrifice, and is this sufficiently important to warrant the more extensive 3-D SAFT computation.

An object sufficiently complex as to provide phase interference between adjacent objects is necessary to assess the effect of these various processing approaches on image resolution. The "Y" pattern as described in the previous section was chosen for this object. A SAFT data file was collected by scanning this object and will serve as the "parent" data file for this study. This unprocessed data file is shown in Figure 3.5. Each processing method will use this file as its original data file.

Table 3.1 shows graphically three separate SAFT processing options that could conceivably be performed to analyze SAFT data. The first two methods are a comparison of 3-D SAFT and Line-SAFT. Line-SAFT is simple to implement on the SAFT-UT system. The aperture definition simply defines a cone with a circumferential dimension of 1. So one would expect a focusing effect in one dimension (x), but no focusing in the other dimension (y). Figure 3.6 shows an image of the full 3-D SAFT processing of the chosen "parent" data file.

0011

BEST COPY AVAILABLE

TABLE 3.1. Flow Diagram of Three SAFT-UT Processing Options

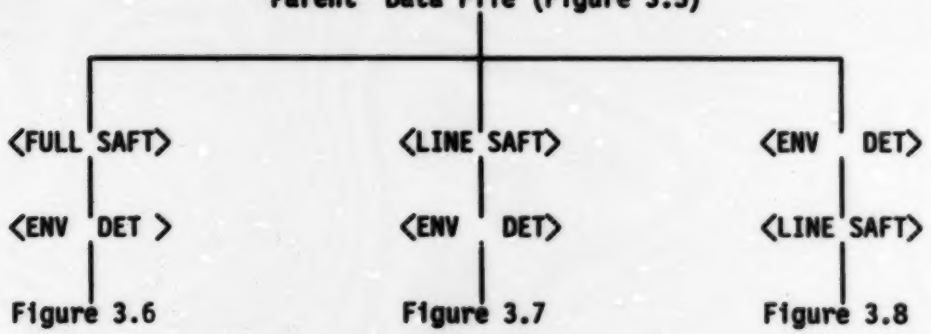

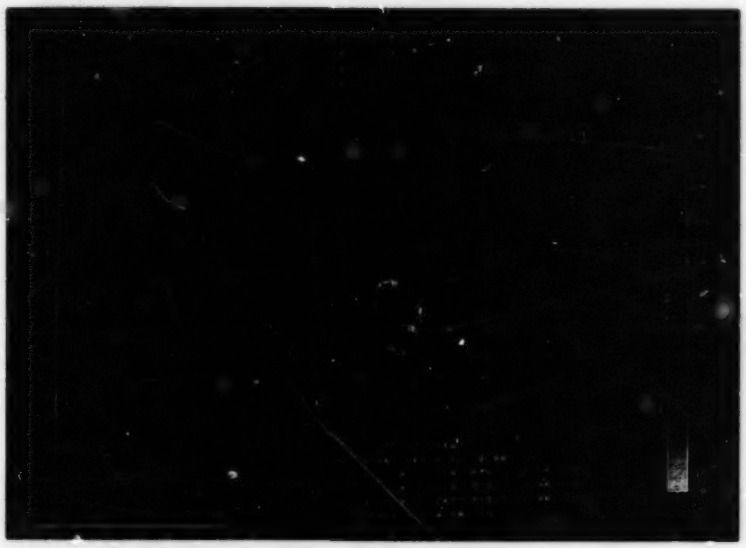

FIGURE 3.5. "Parent" Unprocessed "Y" Pattern Data File

The flat-bottom holes are well focused and distinguishable in all dimensions. Figure 3.7 shows the Line-SAFT result of the same "parent" data file. A significant image degradation occurs and the holes are totally indistinguishable. In this complex geometry full 3-D SAFT proves to be much superior to Line-SAFT.

The final processing technique investigates the possibility of processing low-frequency, video-detected signals instead of the undetected rf signal. If this method would prove to be successful, then the data could be envelope detected prior to digitization and a much lower sampling frequency could be used to fully describe the waveform, since the signal would contain much lower frequencies. Thus, a much faster processing rate could be realized simply because there is less data to process. Figure 3.8 shows the result of SAFT processing the data file after it has been envelope detected. Notice there

0012

BEST COPY AVAILABLE

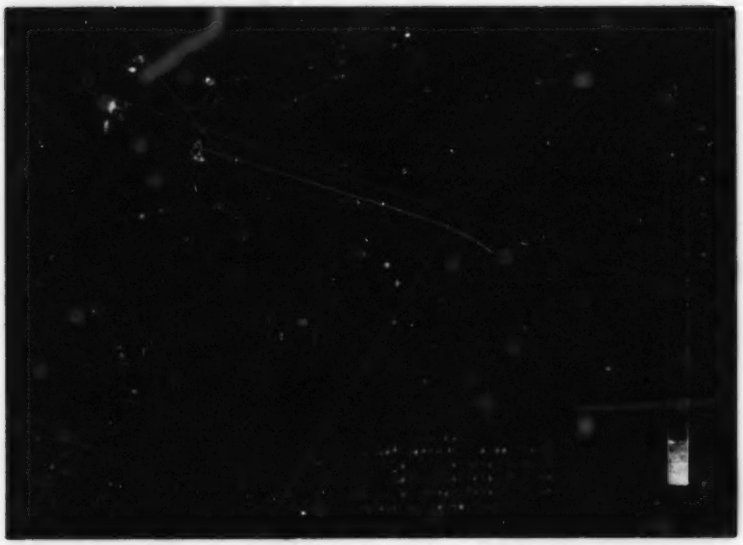

FIGURE 3.6. Full 3-D SAFT Reconstruction of the "Y" Pattern Data File

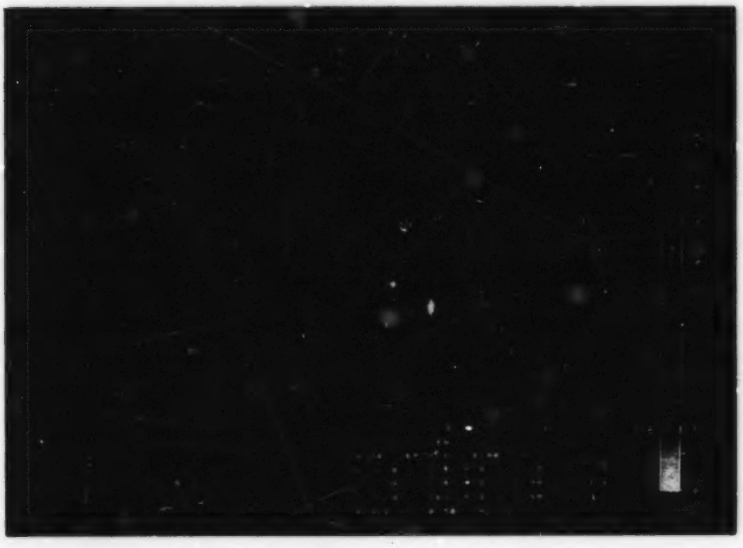

FIGURE 3.7. LINE-SAFT Reconstruction of "Y" Pattern Data File

is no focusing effect on individual holes, but rather the phase relationships have been destroyed and thus the focusing occurs as if the "Y" was one continuous object.

BEST COPY AVAILABLE

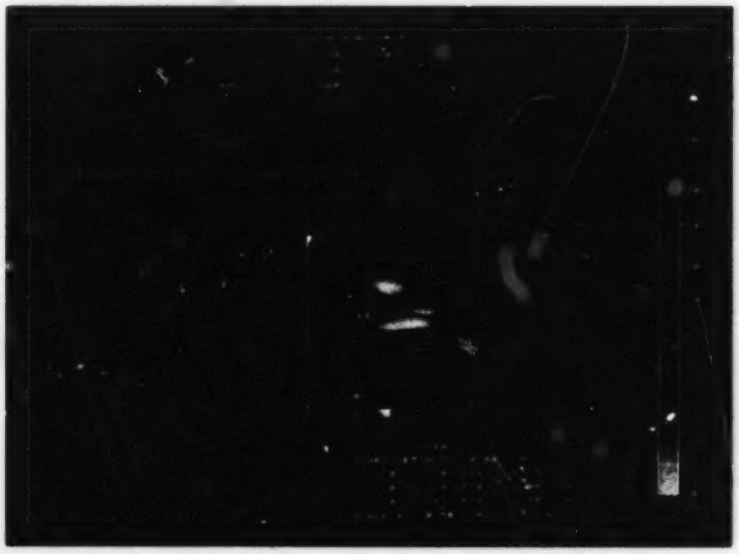

FIGURE 3.8. LINE-SAFT Reconstruction Subsequent to Envelope Detection of the "Y" Pattern Data File

Finally, a conclusion from this study may be made. For complex volumetric defects, one may declare the 3-D SAFT technique significantly superior in imaging quality (better resolution) but all should successfully detect the defect. Alteration of the 3-D SAFT algorithm to utilize the alternate methods presented here, then, would reduce the information presented to the operator and significantly impair his ability to size and characterize defects of interest.

3.3 TSAFT VELOCITY AND THICKNESS VARIATION STUDY

Two performance evaluation studies were focused on the TSAFT configuration to determine the sensitivity of this mode to velocity errors and thickness measurement errors. It was also a goal of these studies to determine the degradation that occurs due to these variations.

The basic assumption of the SAFT algorithm is that it assumes isotropic and homogeneous material with respect to velocity; that is, the calculations performed by the SAFT processing makes the approximation that the velocity is constant throughout the material. This, of course, is not exactly true in most specimens; and the variance depends greatly on the type of material under test. Also the algorithm requires that the velocity be known to some degree of accuracy. This may seem to be a trivial requirement, but in fact in many cases it is not. For example, an extreme case is CCSS material, which varies in velocity as a function of angle in the material. The following, then, is an experimental study to determine the image effects of erroneous velocity measurements on TSAFT data files.

0014

BEST COPY AVAILABLE

The data file chosen for this experiment is a TSAFT scan of a 0.3-inch-deep sawcut in 0.585-inch-thick 304 stainless steel material. The material is a flat coupon with actual characteristics that are known very accurately. Each element in the chosen sequence utilizes the same data file, but simply varies the velocity parameter in the data file header block. This simulates choosing an erroneous velocity parameter when acquiring the data.

Figure 3.9 shows the series of images obtained by sequencing the velocity of the material. The known velocity is 122000 inches/ sec for SAFT illumination in the shear mode. Each element in the sequence represents approximately a 10 percent change in velocity. Figure 3.9(a) was processed at 102000 inches/ sec, (b) at 112000 inches/sec, (c) is the actual velocity of 122000 inches/sec, (d) is 132000 inches/sec, and (e) is 142000 inches/sec.

It should be noted that each file was processed to include the complete data; therefore, both the true and conjugate images are visible. Since the object is a semi-circular shaped sawcut, then one would expect the fully illuminated tandem image to be elliptical in shape with its center line located at the back-surface line. When one observes the image using the actual velocity, Figure 3.9(c), this is indeed the case.

The images in the sequence may now be analyzed to determine the major differences that have occurred. The most pronounced effect of velocity differences is shown to be a vertical displacement error. As the velocity increases, it is apparent that the image is mapped deeper into the material. When observing the vertical movement of these images, it can be noted in general, for every 10 percent increase in material velocity, a vertical movement of about 1/4T is realized. This observation is important. It is apparent that TSAFT is very sensitive to velocity errors that primarily result in vertical positional errors.

Another observation can be noted by observing these images. The general image quality and characteristics deviate much less than expected. This is important to consider. Even with dramatic velocity errors, the image integrity is retained with respect to general shape and size features.

Another parameter of the TSAFT that is interesting to study is the measured material thickness. Just as the material is assumed to be homogeneous with respect to velocity, it is also currently assumed to have a constant thickness along the region of illumination, or in other words it assumes that the front and back surfaces are uniform and parallel. This is obviously an approximation, since in many pipe materials shrinkage may occur near the weld area or large counterbore transition regions may be present on the ID surface. For TSAFT especially, one may wonder what effects this will have on the image quality, since TSAFT relies on multiple bounce paths to illuminate the object zone. These paths are assumed to be well known in the image calculation and in fact may not be that well known.

0015

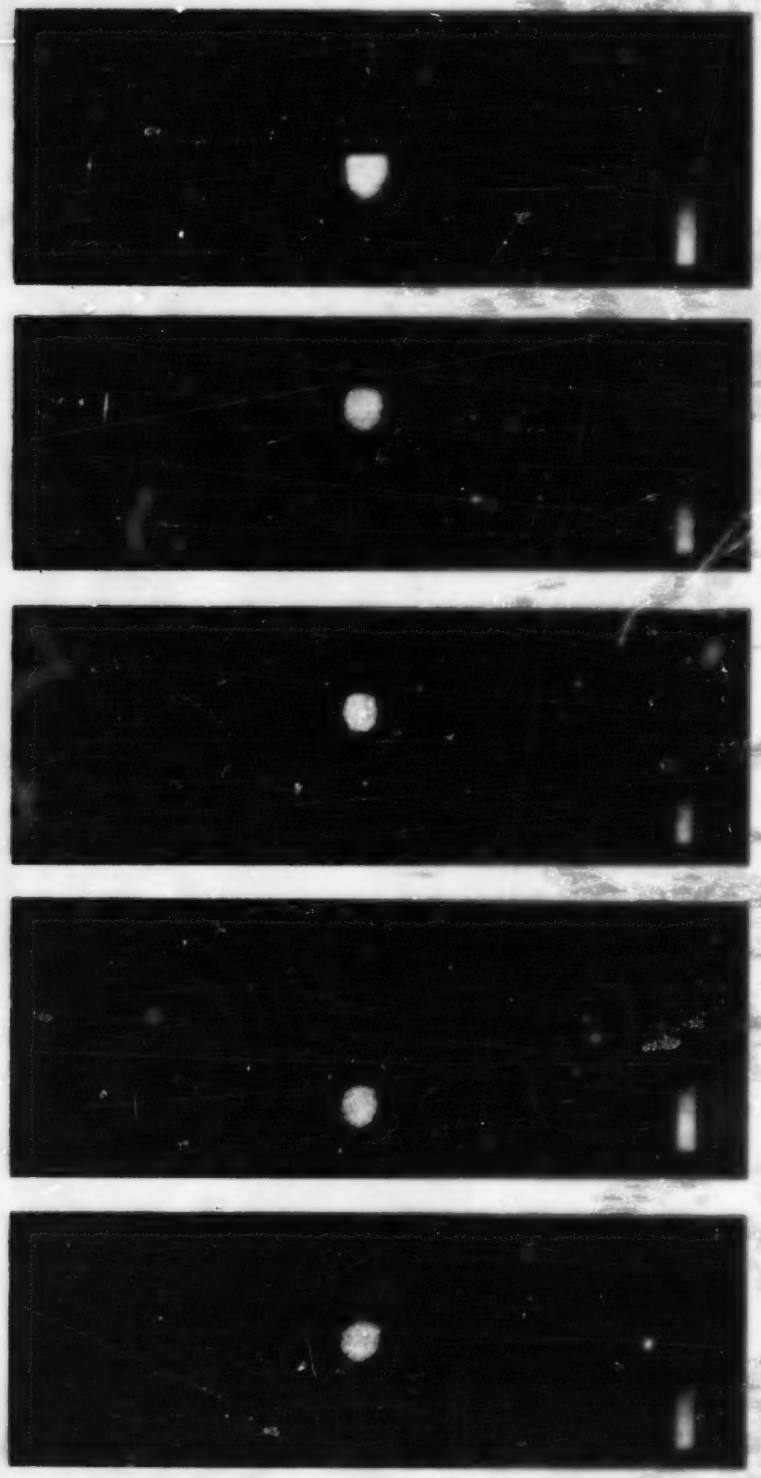

(a) V = 102000 in/sec

(b) V = 112000 in/sec

(c) V = 122000 in/sec

(d) V = 132000 in/sec

(e) V = 142000 in/sec

FIGURE 3.9. TSAFT Velocity Sensitivity Study Sequence

BEST COPY AVAILABLE

Again the data file chosen for this experiment is the TSAFT scan of a 0.3-inch-deep sawcut in 0.585-inch-thick 304 stainless steel material. The same data file is used to create the thickness variation sequence, with just the thickness parameter in the data file header adjusted to the appropriate value. This should accurately simulate separate scans that were acquired using these various thickness values.

The resultant images are shown in Figure 3.10. The sequence contains five images, incrementing the thickness in 10 percent changes. Figure 3.10(a) shows the image representing a thickness of 0.468 inches, (b) 0.527 inches, (c) the correct thickness value of 0.585 inches, (d) 0.644 inches, and (e) 0.702 inches.

As the assumed thickness is increased, one can observe from these images that the algorithm maps the result more shallow in the material. The characteristics of thickness deviation are very similar to velocity deviation and this should not be too unexpected, since both parameters directly effect where the algorithm predicts the time of flight of a given signal.

As stated previously, the vertical placement of the resulting image is dramatically affected by deviations of either thickness or velocity from the true values of the specimen under test. However, the encouraging result is that the general image integrity is retained. Thus, with the complement of both pulse-echo and tandem scans of the same region a judgement of size and location may be made. The pulse-echo corner-trap image may be used to position the defect laterally and size the length defects, and the TSAFT image may be used to determine the horizontal and vertical extent of the defect. The characteristics of both files may be used to verify the integrity of the other.

3.4 SAFT-UT IMAGING OF NON-VERTICAL DEFECTS

The effects of SAFT-UT imaging of non-vertical defects were studied. A total of six 1.0-inch-thick aluminum test blocks were made, each having an 0.3-inch deep, semi-circular sawcut, but differing in the angle of the sawcut relative to a perpendicular line to the back surface. The angles studied were 0, 5, 10, 15, 20, and 35 degrees. The 0° sawcut was considered the reference block and was scanned using the pulse-echo SAFT, TSAFT, and TSAFT-2 configurations. The remaining five blocks were scanned from each side of the sawcut also using each scanning configuration. All scans in this discussion were performed with 2.25-MHz, 0.25-inch-diameter, contact-mode transducers. Wedges were selected such that a 42.8° center angle was generated in the aluminum material.

The results of the pulse-echo scans indicated that the image of the corner trap echo did not change significantly regardless of the direction the sawcut was tilted or the severity of degree to which it was tilted. The image of the tip-diffracted echo did, however, significantly change. When the sawcut was tilted in the direction of the transducer, the tip indication was also shifted in the same direction and was of a lower intensity value. The converse was true when the sawcut was tilted away from the transducer.

0017

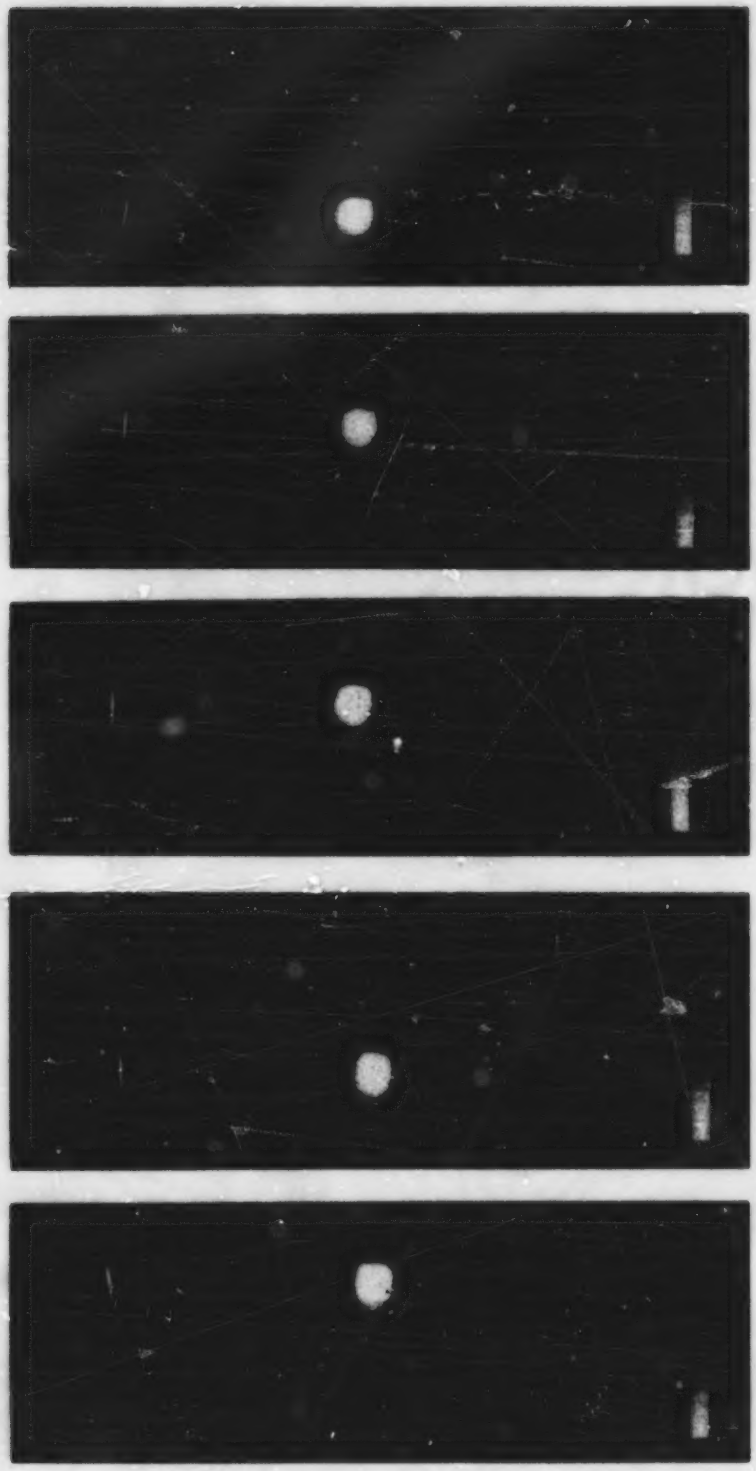

(a) T = 0.468

(b) T = 0.527

(c) T = 0.585

(d) T = 0.644

(e) T = 0.702

FIGURE 3.10. TSAFT Thickness Parameter Sensitivity Study Sequence

0018

BEST COPY AVAILABLE

This effect can be clearly seen when observing Figures 3.11, 3.12, and 3.13. Figure 3.11 shows an image of the 0° sawcut. The tip and corner trap signals can clearly be observed. The displayed images include signals that appear to lie beyond the far-surface (dashed) line. This area is included in order to observe the reflections that occur due to the smooth mirror-like characteristics of the far surface. Figure 3.12 shows the image obtained from the sawcut slanted away (+ direction) from the scanning mechanism by 35°. Notice that the tip signal is greatly enhanced since the reflector is approaching being normal to the 45° illumination angle; and thus, more energy is returned from the reflector face. Figure 3.13 shows the SAFT image of the sawcut slanted 35° toward (- direction) the scanner. As expected, the tip signal amplitude is similar to the 0° image in Figure 3.11, since the reflection is totally due to the diffraction effects of the sawcut edge.

FIGURE 3.11. SAFT-UT Pulse-Echo Image of Vertical Sawcut

Figure 3.14 graphically illustrates the SAFT pulse-echo signal response. This is a graph of peak signal response for the various slanted sawcuts. The corner-trap signal is maximum at 0° and tapers off as the slant angle is altered. However, around -15° and +10°, a nulling effect can be observed. This apparently is due to phase cancellations that occur at these angles since multiple sound paths are contributing to the corner-trap response.

The lower curve in Figure 3.14 represents the peak response observed from the tip signals of the slanted sawcuts. Notice that the curve has a crest at -10° and begins to drop off until about +10°. The curve from -35° to +10° is the tip-diffracted signal response, with variations due to varying path-length (attenuation) and higher order effects. At +10° the energy from the planar face of the sawcut begins to dominate the signal response, and a marked increase in signal can be seen at angles greater than +10°. If one

BEST COPY AVAILABLE

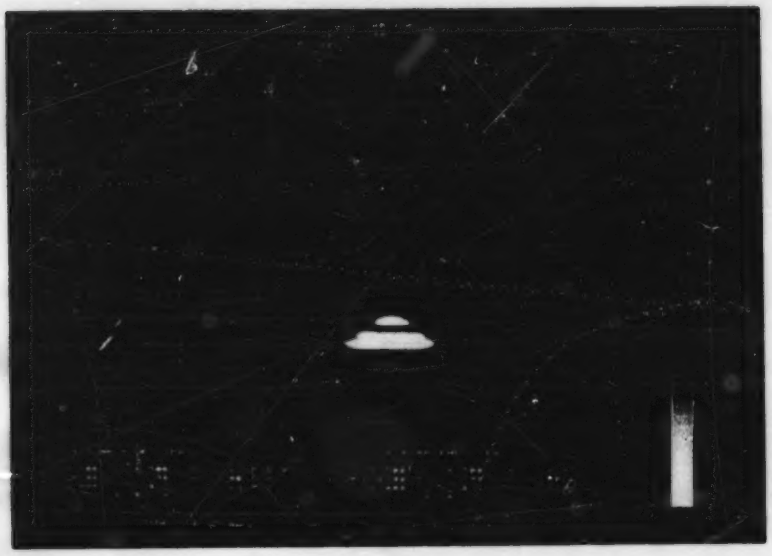

FIGURE 3.12. SAFT-UT Pulse-Echo Image of a +35° Slanted Sawcut

FIGURE 3.13. SAFT-UT Pulse-Echo Image of a -35° Slanted Sawcut

0020

BEST COPY AVAILABLE

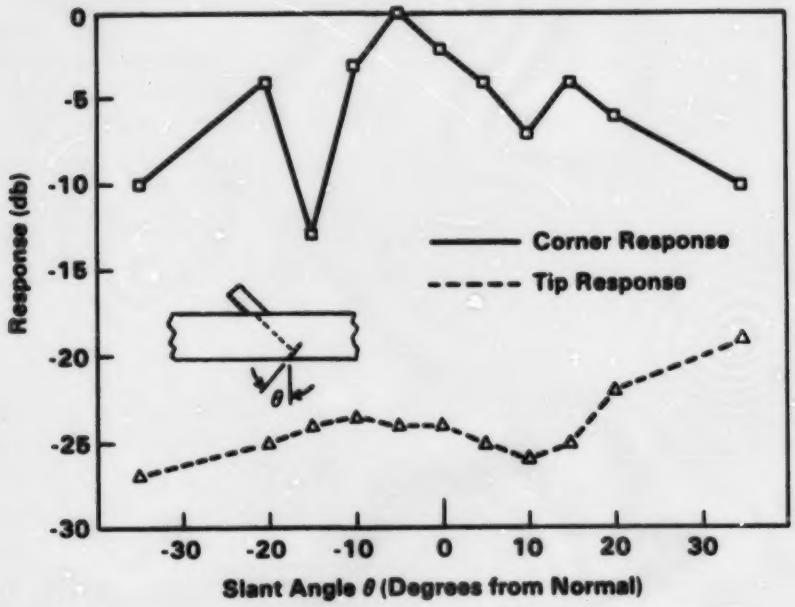

FIGURE 3.14. SAFT-UT Pulse-Echo Configuration Peak Signal Response vs. Machined Defect Slant Angle

were to extrapolate both curves in Figure 3.14 to a fictitious +47.2° sawcut (normal to the inspection angle of 42.8°), the two curves should intersect as the full face of the sawcut is directly seen by the transducer.

When considering the effects of defect orientation in the tandem configurations, it is helpful to first investigate the signal response for these configurations. Figure 3.15 shows the peak signal response for various non-vertical sawcuts. One curve represents data observed with the transmitter always set 3/2 Vee from the base of the reflector. The receiver was then adjusted to obtain the maximum value that was recorded. This "fixed-transmitter and adjusted-receiver" curve represents the TSAFT case. The second curve in Figure 3.15 was collected by placing the receiver at the peak pulse-echo response location and subsequently adjusting the transmitter to produce the peak reflector response. This configuration closely resembles that which would be expected from the TSAFT-2 case. Note that for both cases, the curve characteristics are very similar to the pulse-echo corner-trap response previously discussed in Figure 3.14; phase cancellation nulls occur around angles -10° and +10°. This is to be expected since the tandem configurations are taking advantage of the back-surface reflection mechanism inherent in the pulse-echo corner-trap.

When one analyzes the TSAFT and TSAFT-2 imaging characteristics, one would expect that the peak raw signal response curves would contribute to the overall processed image dynamic range. Figure 3.16 shows that this is indeed the case. This graph shows the maximum value in the corresponding processed

BEST COPY AVAILABLE

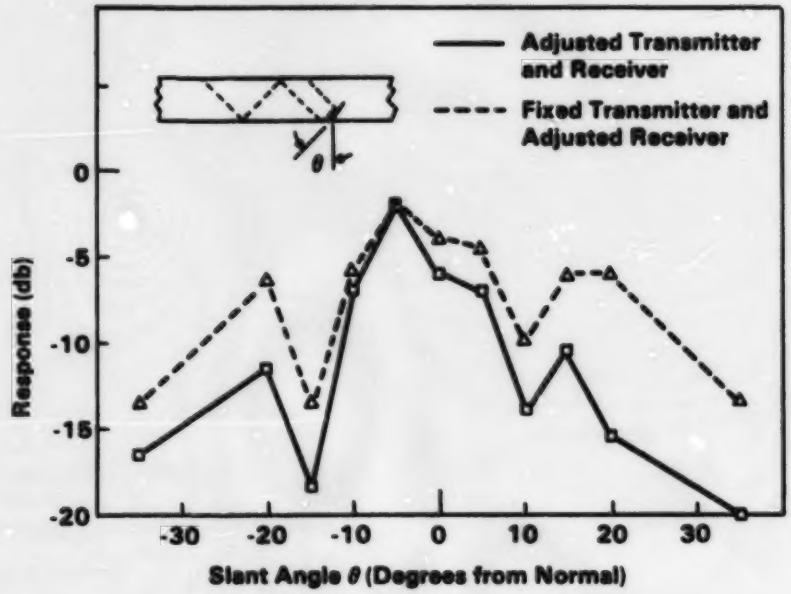

FIGURE 3.15. SAFT-UT Tandem Configuration Peak Signal Response vs. Machined Defect Slant Angle

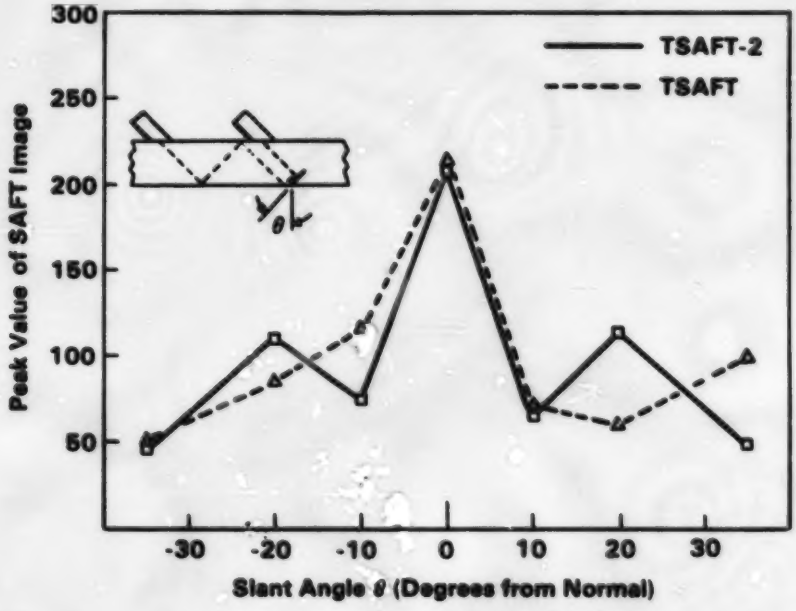

FIGURE 3.16. TSAFT and TSAFT-2 Configuration Image Maximum Value vs. Machined Defect Slant Angle

BEST COPY AVAILABLE

image for sawcuts with varying slant angles. The TSAFT-2 plot more closely resembles the peak signal responses of Figure 3.15, with nulls occurring at -10° and +10°. The TSAFT curve on the other hand shows that this processing tends to smooth the curve somewhat. The variations of these curves relative to the signal peak response is due to the fact that SAFT processing sums contributions from multiple angles to produce a given processed data point. Therefore, the result is a product of multiple contributors with angles deviating from the center angle.

The logical next step is to observe the sizing characteristics of TSAFT and TSAFT-2 as planar reflectors deviate from the vertical orientation. Figure 3.17 shows the TSAFT image of the +10° slanted sawcut. Notice that at the far-surface dotted line there is a strong indication due to edge diffraction from the intersection of the far surface with the defect. The planar surface also

FIGURE 3.17. TSAFT Image of +10° Slanted Sawcut

produces a significant indication of the upper structure at this angle. However, in the TSAFT mode, the sawcut conjugate image is weak. This would normally appear below the dotted far-surface line; but, because of the extended path lengths of the conjugate image in the TSAFT configuration, it does not appear in this image. Figure 3.18 shows the TSAFT-2 image of the identical +10° slanted sawcut. Notice that the illumination is much improved over the TSAFT image. The indication from the far-surface intersection is strong, and both the true image and the conjugate image are well represented. This is due to the fact that all center ray path lengths are constant for a given vertical plane in the TSAFT-2 configuration. Also comparing the TSAFT-2 image with the TSAFT image there is an apparent vertical resolution improvement; each

0023

BEST COPY AVAILABLE

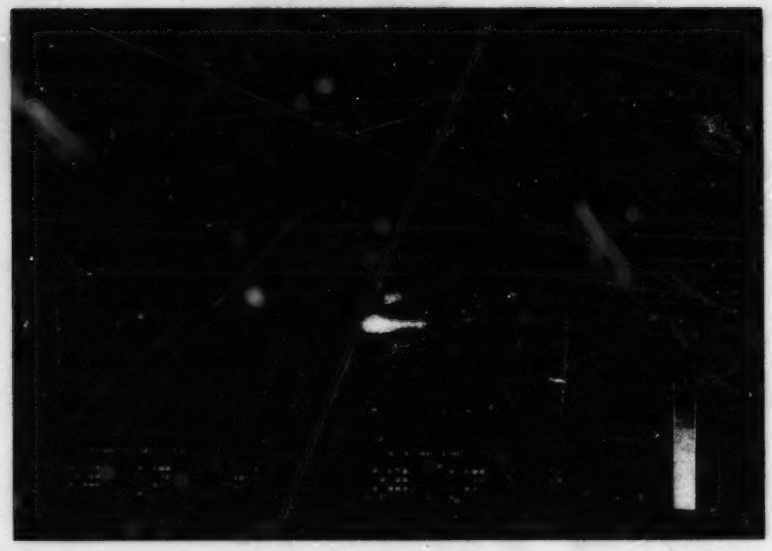

FIGURE 3.18. TSAFT-2 Image of +10° Slanted Sawcut

feature is more sharply imaged. This is due to the fact that TSAFT is a fixed-transmitter, scanned-receiver configuration; while TSAFT-2 is a simultaneous source/receiver scanned configuration. In theory TSAFT-2 should provide a factor of two image-resolution improvement over TSAFT in the axial direction, which corresponds to a vertical improvement of approximately a factor of $[2 - \cos(A_i)]$, where A_i is the illumination angle. So for 42.8° illumination, an improvement of 1.3 can be expected in the vertical direction.

As the machined defect is tilted further, the indication from the planar surface dramatically reduces in intensity. Figure 3.19 shows the TSAFT image of a 20° slanted sawcut. A strong indication is apparent from the sawcut far-surface edge, but the upper structure of the sawcut is not imaged at all. Figure 3.20 shows the TSAFT-2 image of the same sawcut with similar results. The resolution effects discussed earlier are apparent when comparing these images. The edge feature (a line reflector) is smaller in the vertical direction in the TSAFT-2 image than in the TSAFT image.

When determining the vertical extent of an indication from a surface-connected defect, the full tandem image is presented on the display screen. This includes the mirror or conjugate image that appears beyond the far-surface dotted line. The full image, including the conjugate, is measured in the vertical direction; and this value is then halved. This method reduces the sensitivity of the measurement to material thickness and velocity parameters. Particularly in a weld region, the material depth at the weld root may not be the same as the parent material thickness; so the dotted line becomes a general indication of where the far surface is expected in the image. A sizing method incorporating the far-surface line, then, would increase the necessity to know this value more accurately; and in many cases, it is not well known.

0024

BEST COPY AVAILABLE

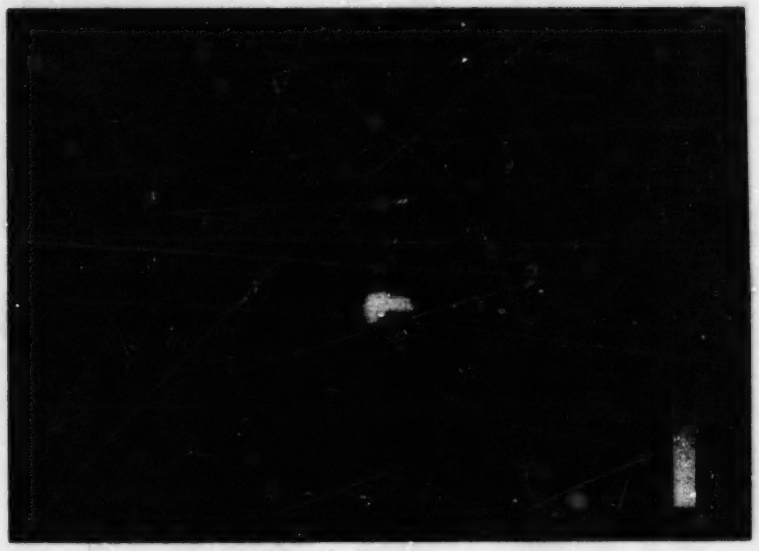

FIGURE 3.19. TSAFT Image of +20° Slanted Sawcut

FIGURE 3.20. TSAFT-2 Image of +20° Slanted Sawcut

BEST COPY AVAILABLE

Two sizing criteria were used in the tandem vertical sizing study. These were -3 db and -6 db levels relative to the maximum value of the image. The operator measured the vertical distance of the indication that extended between the appropriate level. Figure 3.21 shows the results that were obtained from the TSAFT processed images; and correspondingly, Figure 3.22 shows the results from the TSAFT-2 images. The -6 db criterion will be discussed here, since this is what we have been using, except for situations which have high noise levels.

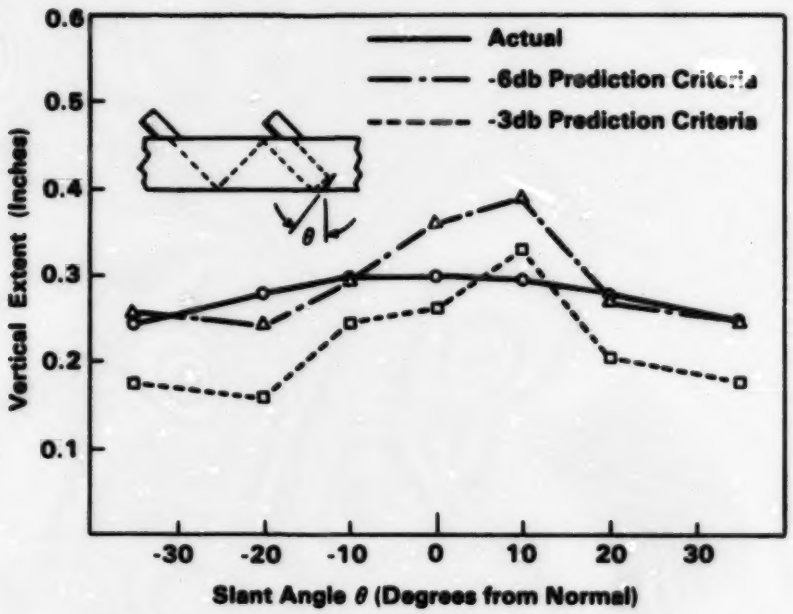

FIGURE 3.21. TSAFT Vertical Prediction vs. Machined Defect Slant Angle

From the previous discussion, the range of slant angles that includes any upper structure information is from -10° to +10°. Outside this range, the sizing criterion is only really measuring the height of the indication from the far-surface intersection edge and no vertical information is present in the signal. These larger angle values do give an indication of the resolution of the configurations. The edge can be considered to be a line reflector, and therefore the size measured in angles greater than 10° and less than -10° can be used to define the vertical resolution of the particular configuration. Notice the resolution of the TSAFT configuration is about 0.16 inches at -3 db, and for TSAFT-2 the vertical resolution is about 0.11 inches at -3 db. This is a ratio of 1.4, which is close to the previously predicted improvement of 1.3 from the TSAFT-2 configuration relative to the TSAFT configuration. Also, remember that this data is from transducers with diameters of 0.25 inches.

BEST COPY AVAILABLE

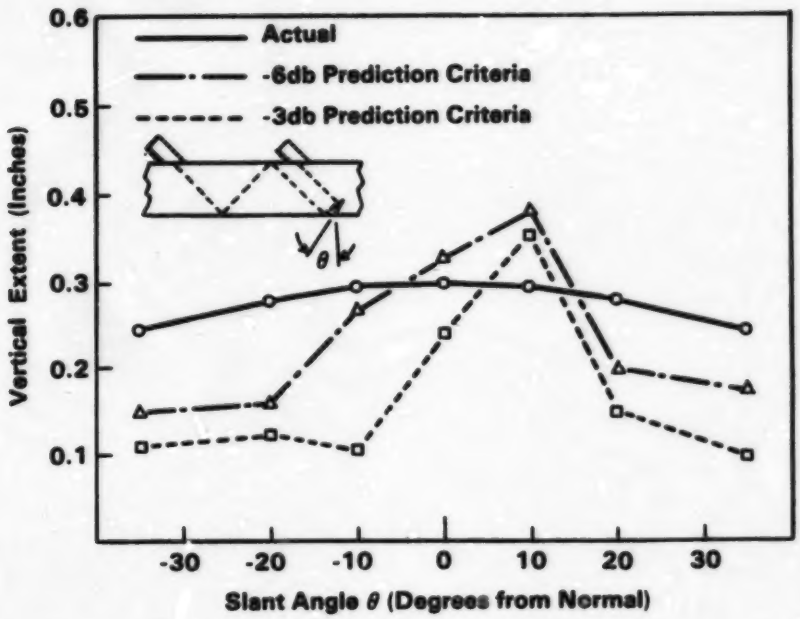

FIGURE 3.22. TSAFT-2 Vertical Position vs. Machined Defect Slant Angle

The TSAFT and TSAFT-2 results provide reliable and accurate sizing information between -10° and +10°. Outside of this slant angle range for smooth planar reflectors, the tandem configurations provide degraded sizing information because less energy from the planar surface is returned to the receiver.

3.5 TSAFT AND TSAFT-2 SIZING PERFORMANCE ON MACHINED VERTICAL SAWCUTS

Further tests were made to determine the accuracy of sizing defects using the TSAFT and TSAFT-2 configurations. Ten vertical sawcuts ranging from 0.050 to 0.700-inches deep were placed in 0.75-thick aluminum material. Transducers with center frequencies of 2.25 MHz and diameters of 0.25 inches were used. These were implemented in the contact mode, and the 45° shear mode was utilized.

After processing the data, two sizing criteria were used for determining the vertical extent of the image. These utilized levels of -3 db and -6 db. As stated previously, the operator measured the vertical distance of the indication that extended between the appropriate level. Since the image contains both the real image and the conjugate image, this value is halved to obtain the final result.

Figure 3.23 shows graphically the results obtained with the TSAFT configuration. And correspondingly Figure 3.24 shows the results with TSAFT-2. If one examines the -6 db curve in Figure 3.23, it can be seen that TSAFT, in this range of defects, tends to oversize by approximately 0.050 inches. And in Figure 3.24, it can be seen that TSAFT-2 provides an improved accuracy. This is expected, since as stated previously, TSAFT-2 exhibits an improved

BEST COPY AVAILABLE

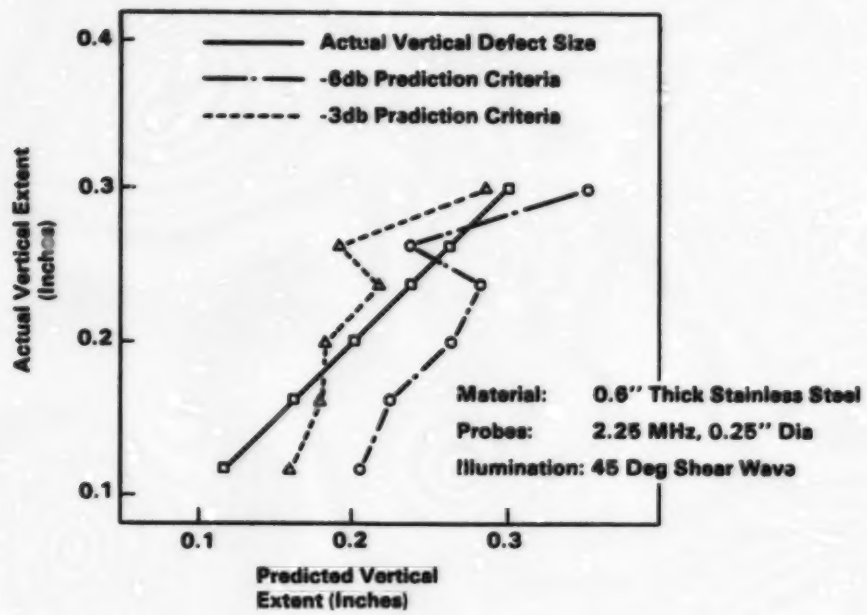

FIGURE 3.23. TSAFT Vertical Prediction vs. Machined Defect Size

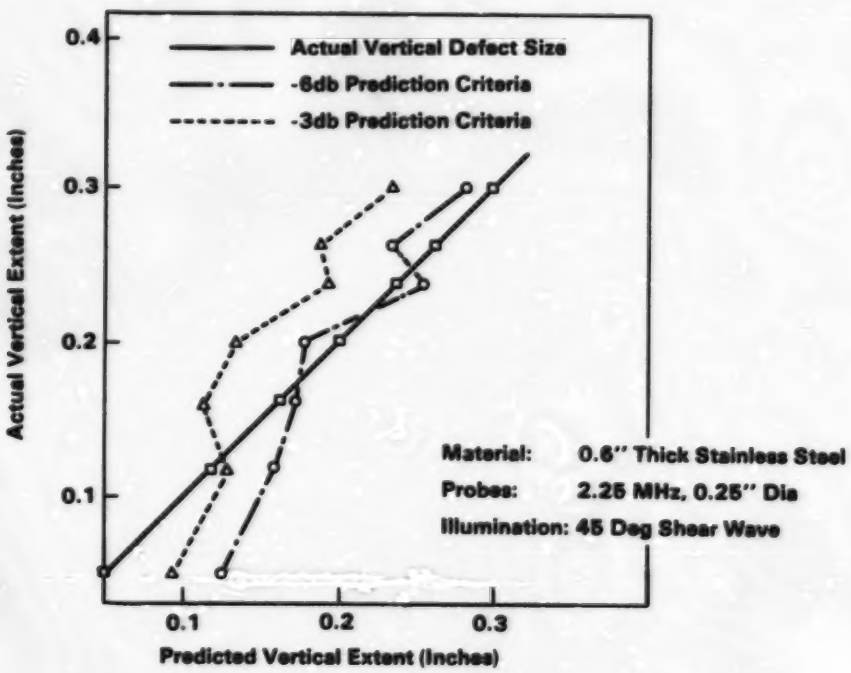

FIGURE 3.24. TSAFT-2 Vertical Prediction vs. Machined Defect Size

BEST COPY AVAILABLE

resolution due to the characteristics of the simultaneous source-receiver scanned configuration which improves the object plane illumination.

Further analysis of Figure 3.24 reveals that the small 0.050-inch deep defect begins to appear as a line reflector. When discussing Figure 3.22, it was learned that the 2.25-MHz, TSAFT-2 system implemented here exhibited a 3-db resolution value of approximately 0.11 inches (2 wavelengths). This is the minimum depth value one would expect to assign from the processed image of a strong line reflector, such as a corner or far-surface intersection. Implementation of smaller probes would reduce the system f-number, which would increase the effective SAFT aperture, and thus improve the resolution performance. Probe center frequency and bandwidth also effect the observed imaging performance. Decreasing the f-number, increasing the center frequency, and increasing the bandwidth however tend to decrease the system signal-to-noise ratio. Configurations for given applications, therefore, should be optimized to produce the best system resolution and signal-to-noise ratio balance.

0029

4.0 REAL-TIME SAFT PROCESSOR DEVELOPMENT

There were three major subtasks worked on over the past year concerning the Real-Time SAFT Processor. These subtasks were:

1. Upgrading the pulse-echo implementation to calculate the complete aperture definition look-up table prior to entering the SAFT inner loop. This reduces the overhead in the total computation and improves performance.

2. Implement the TSAFT/TSAFT-2 algorithm on the real-time SAFT processor.

3. Implement faster 68020 slave cards to achieve improved slave performance.

The first subtask required the addition of a 1-Mbyte global memory board (bringing the unit's total memory size to 2 Mbytes), and modification of the method for calculating the look-up tables was also performed. A 20 to 30 percent increase in overall performance was realized with this effort. This was completed in the first half of the fiscal year.

Implementation of TSAFT on the real-time SAFT processor is defined as Subtask 2. This was expected to be a relatively major effort, utilizing the pulse-echo software already developed for its foundation. This has expedited the TSAFT implementation, since much ground has already been covered implementing the pulse-echo algorithm. Subtask 2 is approximately 75 percent complete.

The third subtask included acquiring a single 68020 card and evaluating its performance and, from this, predicting the performance improvement when ten slave cards are implemented. The newer cards are expected to provide a speed improvement of approximately 2.5 and expand the local memory for each slave card from 0.5 Mbytes to 1.0 Mbytes. The memory expansion will allow for much larger data files and facilitate tandem implementation.

Tables 4.1 and 4.2 show the outcome of an expected performance study using the full complement of ten slave processors in the developed peripheral device. There are four case studies involved in this analysis. The first two cases are files collected on thin material (less than 2 inches). Case 1 is data collected on the Materials Reliability Center (MRC) stainless steel pipe sample, 1.25-inches thick. This file is characteristic of actual data collected for detection of IGSCC in reactor piping. There are 2501 A-scans in this file with 325 samples each. The Case 2 file contains data collected on a 0.585-inch-thick stainless steel coupon with a 0.3-inch-deep machined defect placed in it. It has 2880 A-scans that are 327 points long.

Files containing data from thicker materials are represented in Cases 3 and 4. Case 3 is data collected from a PISC-II steel block that had a thickness of ten inches. There are 3111 A-scans of 853 points each in this data set. Case 4 contains data from an aluminum resolution block that contains flat-bottom-drilled holes in a "Y" pattern. This data file has 900 A-scan with 1024 points each.

BEST COPY AVAILABLE

Tables 4.1 and 4.2 show the estimated speed of the completed real-time SAFT processor based on timing runs performed on a single 68020 slave board. Table 4.1 contains the results utilizing the SAFT-UT selective processing technique at a threshold level of -20 db. Table 4.2 shows the expected performance without implementing this technique. The tables indicate both the elapsed processing time and the rate indicated in units of A-scans per second. The goal that has been set is to perform SAFT processing at the rate at which data is being collected, which has been set to the value of 10 A-scans/second. These tables show that this goal is expected to be met on the materials provided. Comparing Tables 4.1 and 4.2, a speed improvement of 13 percent to 253 percent is observed, depending on the characteristics of the particular data file.

A full complement of ten slave cards are expected to be purchased and installed during the next fiscal year.

TABLE 4.1 Estimated Real-Time SAFT Processor Performance (-20 db Selective Processing Implemented)

	Elapsed Time, min.	Rate (A-scans/sec)
CASE 1	1.18	35.2
CASE 2	1.78	23.9
CASE 3	4.88	10.6
CASE 4	1.42	10.6

TABLE 4.2 Estimated Real-Time SAFT Processor Performance (No Selective Processing Implemented)

	Elapsed Time, min.	Rate (A-scans/sec)
CASE 1	1.66	25.0
CASE 2	2.01	23.8
CASE 3	17.30	3.0
CASE 4	3.50	4.3

0031

5.0 SAFT-UT DATA COLLECTION AND ANALYSIS

A variety of specimens were studied during the past year. The significant purpose of this effort has been to generate an engineering data base for the SAFT-UT technology and to gain valuable experience on actual samples. This work will assist in establishing a code case for SAFT-UT technology and developing appropriate test and analysis procedures for future uses of this technology. The data collection and analysis consisted of: NAVSEA block data collection and analysis, Materials Reliability Center test stands, SAFT-UT data collection and analysis on KAPL specimens, CCSS data collection and analysis, and Mini-Round Robin IGSCC samples.

5.1 NAVSEA BLOCK DATA COLLECTION AND ANALYSIS[(a)]

A submarine hull weld test specimen was received from AMDATA, Inc. at the end of December 1985. The specimen was one of 18 fabricated specimens representing typical structural welds present on submarines. Specifically, the specimen was originally supplied by General Dynamics, Electric Boat Division, to AMDATA for their inspection; and subsequently transferred to PNL for further inspection using the SAFT-UT imaging system. The following discussion will describe the SAFT-UT system and inspection results concerning this test plate.

Figure 5.1 shows a drawing of the plate that was inspected using the SAFT-UT imaging system including the data acquisition system. Characteristic markings are indicated in this figure with Figure 5.1a showing what will subsequently be referred to as the "top" side and Figure 5.1b showing the "bottom" side.

Table 5.1 describes the full set of inspection apertures and configurations utilized for SAFT-UT inspection of this plate. Initially a full inspection was performed to determine general characteristics of the plate and locate particular areas of interest for more detailed inspection. Inspection numbers 1 through 6 represent this set of scans. One particular area of interest was located 13.4 inches along the weld from the edge of the plate with the "eye" welded on it. This edge is utilized throughout this inspection as the circumferential reference location (y=0 location). Gains were set based on reflectors present at the 13.4-inch location, since calibration blocks were not provided. The gain settings for each scan are indicated in Table 5.1 (maximum gain in the current SAFT-UT data acquisition subsystem is 67 dB). The gain setting will affect the sensitivity of this inspection for the detection of smaller defects if they are present in the material. No other areas in the plate revealed reflectors at this sensitivity level. Therefore, subsequent discussion will focus on scans performed about the 13.4-inch location.

(a) The work on the NAVSEA block was financed by Combustion Engineering, Windsor, CT.

0032

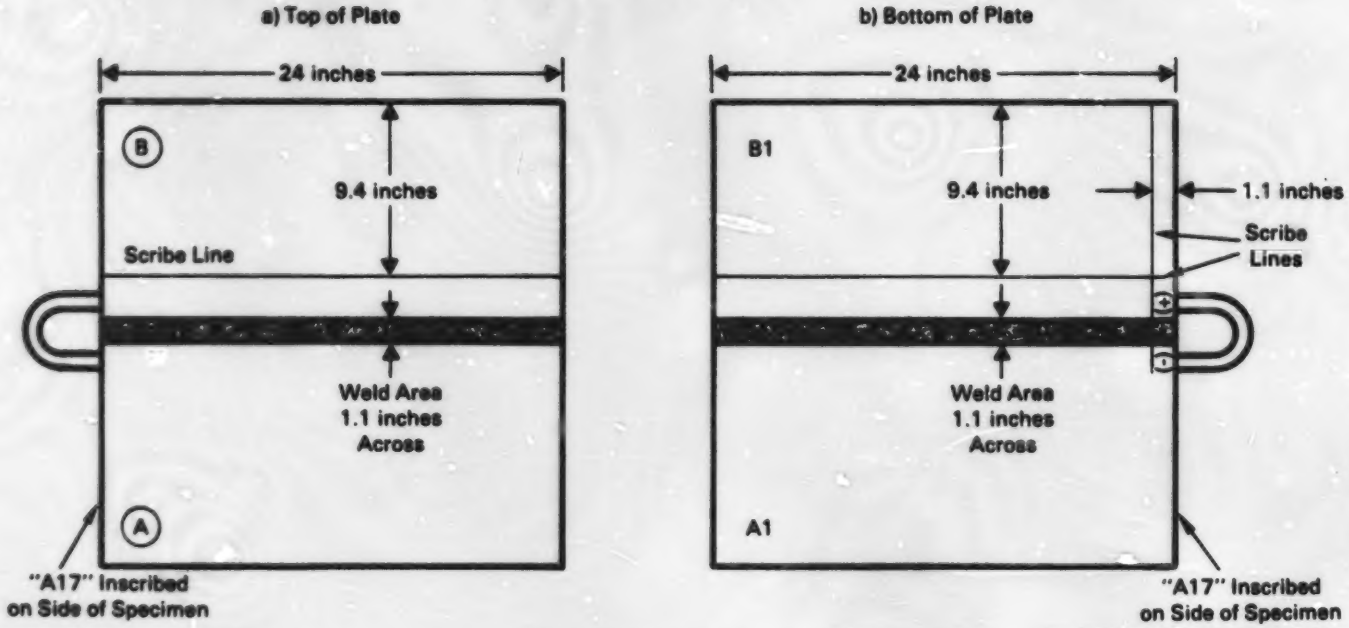

FIGURE 5.1. Dimensions and Reference Lines of PISC II Block Number 2

BEST COPY AVAILABLE

TABLE 5.1. SAFT-UT Inspection Configurations Performed on NAVSEA Test Plate

(PE = SAFT-UT pulse-echo configuration)

Scan No.	Conf	Freq., MHz	Gain, dB	Angle, deg.	Side of Plate	Range, inches Circum.	Axial
1	PE	2.25	46	45	top-A	0.25-10.25	0.55-3.55
2	PE	2.25	46	45	top-B	0.25-10.25	0.55-3.55
3	PE	2.25	46	45	top-A	9.25-15.25	0.55-3.55
4	PE	2.25	46	45	top-B	9.25-15.25	0.55-3.55
5	PE	2.25	46	45	top-A	13.75-23.75	0.55-3.55
6	PE	2.25	46	45	top-B	13.75-23.75	0.55-3.55
7	PE	2.25	46	45	top-A	14.9-17.9	0.55-1.75
8	PE	5.0	44	45	top-A	14.9-17.9	0.55-1.75
9	PE	2.25	57	60	top-A	14.9-17.9	0.60-2.4
10	TSAFT	2.25	60	45	top-A	14.9-17.9	0.55-1.75
11	TSAFT	5.0	64	45	top-A	14.9-17.9	0.55-1.75
12	TSAFT-2	2.25	60	45	top-A	14.9-17.9	0.60-2.85
13	TSAFT-2	5.0	67	45	top-A	14.9-17.9	0.60-2.85
14	PE	2.25	49	45	bot-A	17.9-14.9	0.80-2.8
15	TSAFT	2.25	61	45	bot-A	17.9-14.9	0.80-2.8
16	TSAFT-2	2.25	63	45	bot-A	17.9-14.9	0.80-2.8

A variety of configurations were chosen to investigate the imaging performance and to provide multiple illumination angles for each detected defect. From the top of the plate seven configurations were utilized (scan numbers 7 through 13 in Table 5.1) varying scan technique, frequency of the transducers, and angle of illumination.

B-scan end views and B-scan side views of each image will be presented in this discussion. This presentation provides full lateral and depth information relative to defects encountered in the aperture described. The arrow present in the B-scan side view (on top of the box surrounding the data) indicates the axial position of the center of the weld region. C-scans could be displayed, but traditionally the two B-scans have been used in SAFT work.

Figure 5.2 shows a SAFT single-transducer, pulse-echo image at 2.25 MHz (scan number 7 in Table 5.1). This image reveals a defect located 0.89 inches vertically from the top of the plate, and 0.33 inches from the weld center on the A side. This defect will be referred to as defect number 1 subsequently and is present in the majority of images to be described. Figure 5.3 shows an image of the identical scan, but a 5-MHz transducer was utilized (scan number 8 in Table 5.1).

Figure 5.4 shows the results of a scan performed similar to scan number 7 in Table 5.1, except 60° illumination is employed. Defect number 1 is visible in the lower-left corner of the end-view presentation. Also notice another (defect 2) reflector is revealed with this illumination due to the higher illumination angle. A weld crown existed on each surface of the plate. This

0034

FIGURE 5.2. Pulse-Echo Image from the Top of the Plate at 2.25 MHz and 45° showing Defect Number 1

FIGURE 5.3. Pulse-Echo Image from the Top of the Plate at 5 MHz and 45° showing Defect Number 1

BEST COPY AVAILABLE

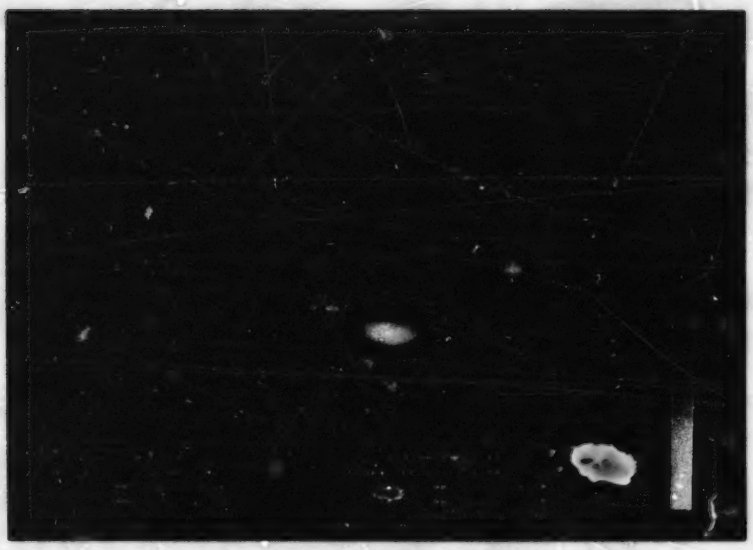

FIGURE 5.4. Pulse-Echo Image from the Top of the Plate at 2.25 MHz and 60° showing Defect Number 1 and Number 2

crown was approximately 1.1 inches across and became an obstacle for the axial scan axis. The 60° configuration was able to illuminate areas closer to the center of the weld than the 45° configuration; and as a result, it detected the second reflector. This defect lies 0.71 inches vertically from the top of the plate, and 0.08 inches from the center of the weld on the A side. The lateral extent of the indication is 0.18 inches.

Figure 5.5 shows a TSAFT view of this area. This scan (scan number 8 in Table 5.1) was taken at 2.25 MHz and 45°. Figure 5.6 shows the same area scanned with a 5.0-MHz transducer and implementing TSAFT also. From this, the vertical and lateral extent of defect 1 can be measured. The defect extends 0.36 inches vertically and 0.46 inches in the lateral direction.

Figure 5.7 shows the results of scanning the area from the top side using the TSAFT-2 configuration at 5.0 MHz. This configuration improves the uniformity of illumination on vertical planes, relative to the TSAFT configuration, and reveals a third reflector near the surface of the plate. The pulse-echo configuration did not detect this reflector due to the proximity of the defect reflection to the near-surface reflection, and the TSAFT configuration did not detect this indication due to the poor near-surface illumination from the source transducer. An advantage of the TSAFT-2 configuration is clearly shown here. It is a valuable technique for detection and characterization of near-surface reflectors as well as uniform illumination throughout vertical planes of the specimen.

BEST COPY AVAILABLE

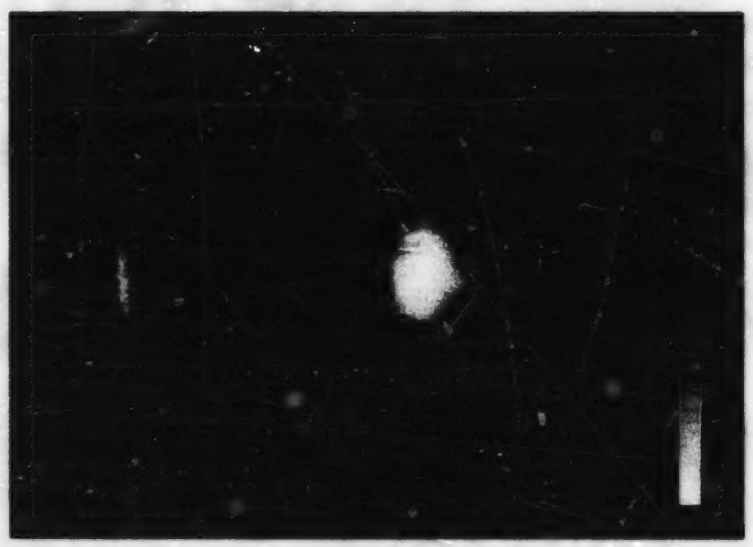

FIGURE 5.5. TSAFT Image from the Top of the Plate at 2.25 MHz and 45° showing Defect Number 1

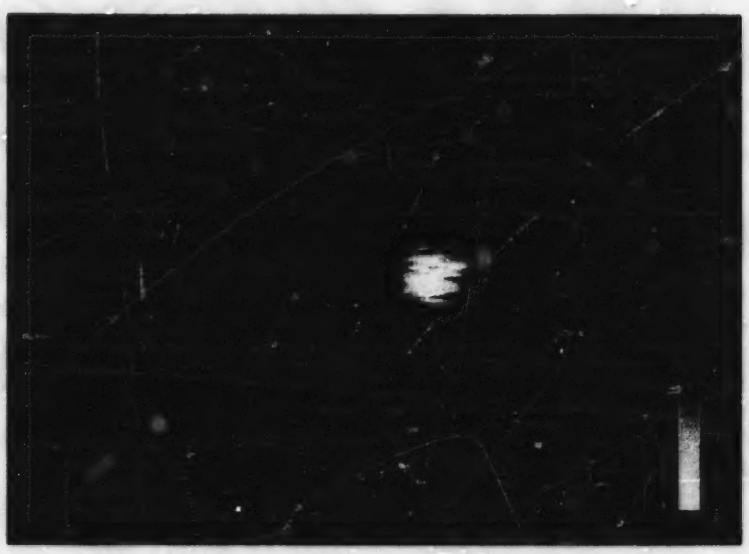

FIGURE 5.6. TSAFT Image from the Top of the Plate at 5 MHz at 45° showing Defect Number 1

0037

BEST COPY AVAILABLE

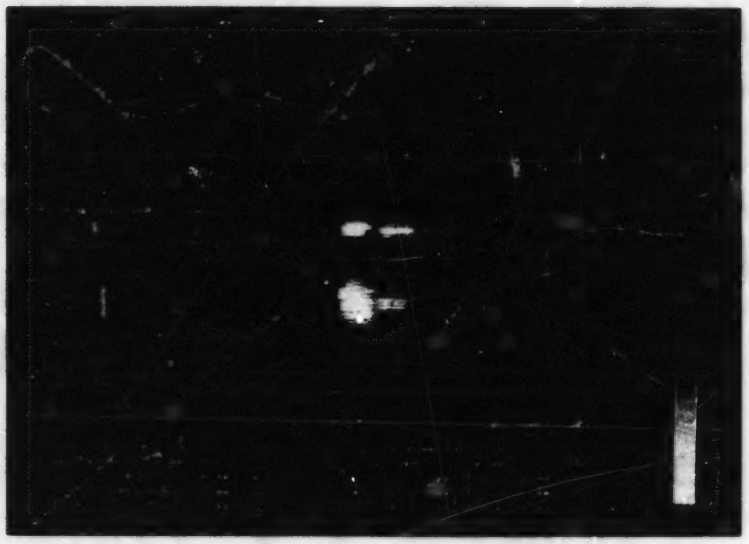

FIGURE 5.7. TSAFT-2 Image from the Top of the Plate at 5 MHz showing Defect Number 1 and Number 3

The existence of defect 3 near the top surface of the plate prompted the desire to perform analysis from the bottom side of the plate to verify the existence of this reflector. Figure 5.8 shows the image of a scan taken on the bottom surface of the plate (scan 14 in Table 5.1). The indication located toward the center of the image is the reflection of defect 1, and the indication located toward the back surface (top of the plate) is the image of defect 3. Figure 5.9 shows a TSAFT image of defect 3.

Table 5.2 shows the sizing and characterization of each of the three defects studied in this report. Defect number 2 was imaged in one configuration only; and therefore, the vertical extent of the defect is difficult to judge. A 6-dB sizing criteria was used to determine the vertical extent of the defects.

TABLE 5.2. Size and Nature of Three Detected Defects in NAVSEA Plate, in.

Defect Number	Vertical Extent from Top of Plate	Circumferential Extent	Position from Weld Center
1	0.89 - 1.10	16.07 - 16.55	0.35
2	N/A - 0.71	17.07 - 17.24	0.10
3	0.24 - 0.77	16.34 - 16.92	0.60

BEST COPY AVAILABLE

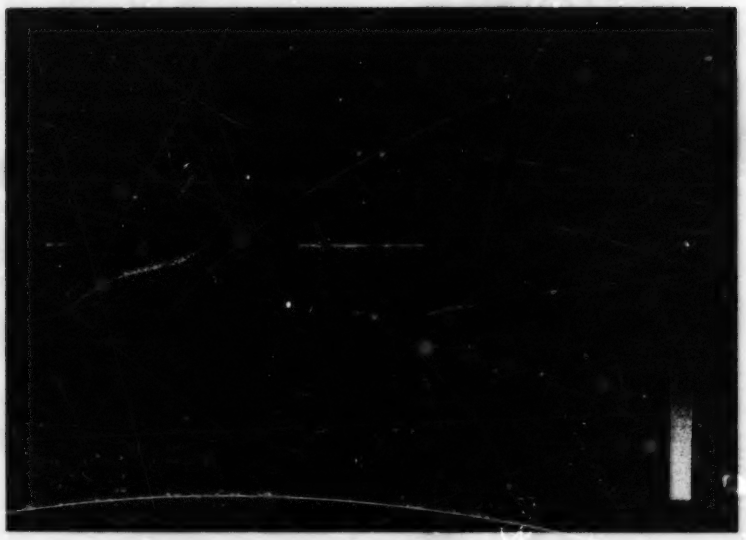

FIGURE 5.8. Pulse-echo Image from the Bottom of the Plate at 2.25 MHz showing Defect Number 1 and Number 3

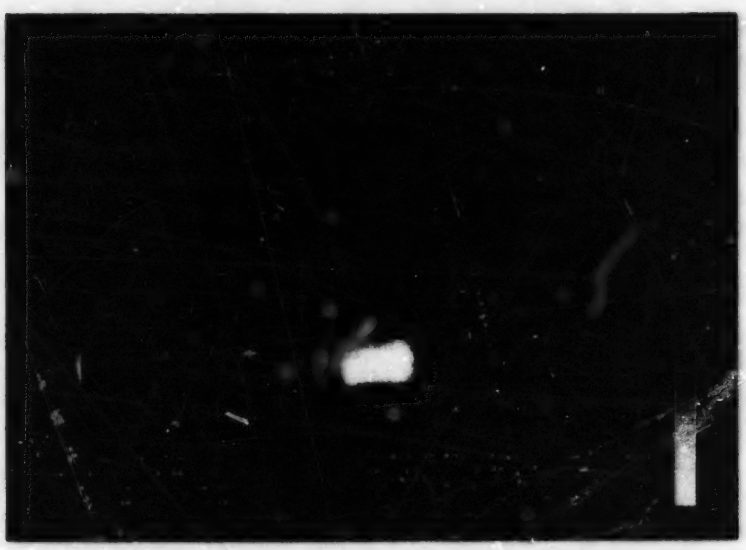

FIGURE 5.9. TSAFT Image from the Bottom of the Plate at 2.25 MHz of Defect Number 3

0039

BEST COPY AVAILABLE

It has been shown in this inspection effort that SAFT-UT provides a comprehensive tool in the inspection of submarine structural welds. It supplies full-volume imaging capability for the sizing and characterization of imbedded defects.

This exercise was the first application utilizing the TSAFT-2 configuration. It proved to supply a substantial improvement in object illumination. It provided a constant illumination of the object area throughout the object plane, and thus near-surface imaging was greatly enhanced.

5.2 MATERIALS RELIABILITY CENTER (MRC) TEST STANDS

In May of 1986 the SAFT-UT field system was transported from the SAFT laboratory in the Physical Sciences Laboratory to the Materials Reliability Center. SAFT-UT data was collected on two test pipes with laboratory-induced IGSC cracking present in three of the four welds. Those test pipes were part of an Electric Power Research Institute (EPRI) program to study IGSCC growth in large-diameter 304 stainless steel piping. In exchange for having access to the IGSCC weldments, the results obtained with SAFT were provided to EPRI. The fundamental objectives of this effort were to:

- Assist MRC personnel in characterizing and sizing defects located at particular areas of interest on these specimens.
- Generate an expanded engineering data base for further development of SAFT-UT technology.
- Provide feedback with respect to SAFT-UT sizing and characterization of actual IGSCC defects.
- Establish optimum procedures and guidelines for SAFT-UT data collection and image interpretation.

The pipes were 24-inch-diameter, Schedule 80, Type 304 stainless steel material. Figure 5.10 shows a sketch of the pipes and the notation that was chosen to reference each weld region. Each pipe was placed vertically in the test stands and contained two welds, which were each given labels that specify the inspection regions. Since there were four welds, there were eight inspection regions given, one on each side of each weld. The circumferential location was measured in inches from a scribe line located in the true north position of each pipe.

The N18/N19 weld contained no defects. It was a Last Pass Heat Sink Weld (LPHSW) and was designed such that under the test loading conditions no cracking should occur. N16/N17 had an overlay placed over a cracked weld. N4/N5 contained a LPHSW after cracking had been initiated. N2/N3 contained cracks in a weld that had no special treatment. SAFT-UT data was collected on the three cracked welds.

0040

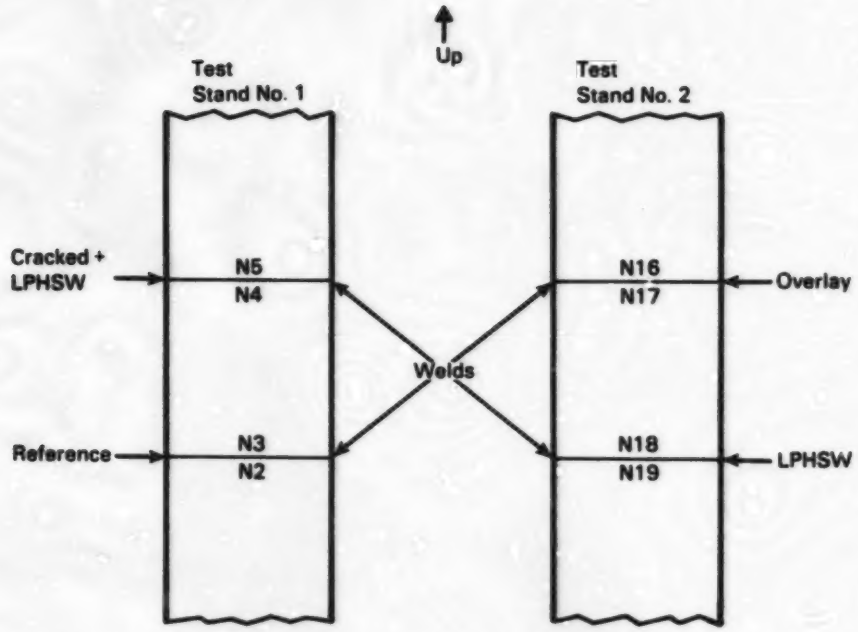

FIGURE 5.10. Test Specimen Configuration

The overlaid weld (N16/N17) was scanned using two configurations for imaging purposes. A pulse-echo single transducer configuration was implemented using 5-MHz longitudinal mode illumination at 43° in the material. This configuration utilized a 0.75-inch-diameter transducer with a 3-inch focal length in a water column stand-off. A tandem SAFT shear-mode implementation using a 50° 1/2-Vee transmitter and 45° receiver was also used. This non-standard tandem configuration was used because the 5-inch width of the weld overlay limited the effective scanning surface. As a result of this constraint, it was not possible to implement the TSAFT-2 configuration.

In addition to these imaging configurations, a normal-beam scan was performed to assist in characterizing the inside-diameter surface of the pipe.

The remainder of the scanning was performed on the N2/N3 and N4/N5 welds. Because no overlay material existed on these welds, they lent themselves to more readily accommodating standard SAFT-UT configurations. Two pulse-echo configurations were implemented for imaging defects in these weld areas. A pulse-echo configuration utilizing a 2.25-MHz, 45°, shear-mode contact probe was first implemented. In addition, the 5-MHz longitudinal pulse-echo configuration previously described for the overlaid weld was also used on the non-overlaid welds.

Both TSAFT and TSAFT-2 configurations utilizing 3/2-Vee illumination were also implemented on these two welds. The tandem scanning included 2.25-MHz, 45°, shear mode with 0.25-inch-diameter contact probes.

0041

BEST COPY AVAILABLE

As with the overlaid weld inspection, a normal-beam scan was also performed to assist in characterizing the inside-diameter surface of the pipe.

A total of six configurations were implemented in the full inspection process. It is appropriate now to discuss the results that were obtained from processing and analyzing this volume of data.

Nine core specimens were extracted from the three cracked welds. Four were taken from the N2/N3 weld, two from the N4/N5 weld, and three cores were taken from the overlaid weld N16/N17. Metallographic sections were prepared from each core specimen to determine actual defect depth.

SAFT-UT data collected on the overlaid weld, N16/N17, proved to be inconclusive with respect to crack depth measurements. The geometries involved prevented SAFT-UT configurations to be implemented that have been designed to facilitate vertical sizing, such as TSAFT-2. The 1/2-Vee tandem configuration that was implemented did not provide satisfactory images. To achieve SAFT-UT imaging with a high degree of confidence level, it is felt that further laboratory study is in order to develop inspection techniques on this class of specimens.

Table 5.3 shows the results obtained from the metallurgical examination of sections of the N2/N3 and N4/N5 welds. These cracks range in size from 0.09 inches to 0.51 inches. Notice there was a machined notch placed in the N4 region. This reflector was 0.10-inches deep and had no cracking extended from it.

TABLE 5.3. Actual Crack Depths from Core Samples

Circumferential Location, in.	Section Label	Crack Depth, in.	
		N2	N3
1.5	A1	0.32	0.09
	A3	0.29	
	A4		0.20
14.0	B1		0.43
	B2		0.41
	B3		0.39
48.0	C1		0.46
	C3		0.48
	C4		0.51
71.0	D1	0.21	0.42
	D3	0.18	0.45
	D4	0.20	0.36

2042

TABLE 5.3. (cont'd)

Circumferential Location, in.	Section Label	Crack Depth, in.	
		N4	N5
15.0	E2	0.10 (notch)	
71.5	F1	0.15	
	F3	0.16	0.09

Table 5.4 gives an overview of the SAFT-UT sizing results obtained on these specimens. There are two columns of SAFT-UT results. The first column are the values initially given to the MRC metallurgical team as preliminary SAFT-UT sizing results. The second column are the values that were obtained from the identical data files, but utilizing analysis techniques learned from this exercise. These will subsequently be discussed on an individual basis.

TABLE 5.4. Comparison of SAFT-UT Vertical Sizing Performance and Actual Measured Crack Depth

(All measurements are in inches.)

Weld Zone	Circumferential Location	Average Metallurgy	Preliminary SAFT-UT	Final SAFT-UT	Final Error
N2	1.5	0.31	. . . did not scan . . .		
	71.0	0.20	0.32	0.28	+0.08
N3	14.0	0.41	0.35	0.33	-0.08
	48.0	0.48	. . . did not scan . . .		
	71.0	0.41	DNSZ*	0.28	-0.13
N4	15.0	0.10 (notch)	0.32	0.20	+0.10
	71.5	0.16	0.34	0.17	+0.01
N5	15.0	0.00	0.39	0.00	0.00
	71.5	0.09	0.47	0.00	-0.09

Mean Error = -0.0157
Standard Deviation = 0.088

*DNSZ = Did Not Size (crack was detected, but no vertical size was reported)

00043

The first line item in Table 5.4 is location 1.5 of weld zone N2. This area was not indicated as a region of interest at the time of data collection; and as a consequence, no SAFT-UT data was taken in this region. The fourth line item, location 48.0 of weld zone N3, was also in this category. They have been included in this table for completeness.

Location 71.0 of weld zone N2 was sized initially using results from both the TSAFT and TSAFT-2 technique. The average of the two results was arbitrarily used as the SAFT-UT sizing value. The final value indicated in Table 5.4 uses the more accurate TSAFT-2 configuration for measuring the vertical extent of the crack. This is also the case for location 14.0 of N3. Since the preliminary SAFT-UT results were given to the MRC team, resolution tests have been performed on these two techniques, showing TSAFT-2 to be more accurate as described in Section 3.5 of this report.

Location 71.0 of weld zone N3 was the most bothersome data-set of the experiment. The metallurgical results indicate there is a significant crack 0.41-inches deep into the material. In this area the SAFT-UT pulse-echo image shows a strong indication from a notch and corner-trap indications from apparent cracking located near the weld material. The TSAFT-2 configuration shows low indications at this point. In the analysis for the preliminary SAFT-UT sizing, these indications were ignored; thus, no defect depth was reported at this location. But when one performs further study of the TSAFT-2 image, this was a judgement oversight. The low-level signal may be due to severe geometry conditions (e.g. counter-bore or shrinkage) or to an error in the data collection process. This is impossible to determine at this point since the region cannot be rescanned. However, improved data collection procedures that were established from this experiment are expected to eliminate the occurrence of this kind of oversight.

Location 15.0 of the N4 weld zone contained an 0.10-inch-deep notch. It was thought that cracking may have been initiated from this notch, thus motivating a metallurgical analysis of this region. After sectioning the sample, it was determined that no cracking had occurred. The defect depth, then, is simply the depth of the notch. However, the preliminary SAFT-UT sizing had specified that the defect depth was 0.32-inches deep. This was disturbing since a 0.22-inch error was realized on a relatively ideal reflector. Further analysis showed that the tandem SAFT data had been collected at a gain established in regions of cracking to maximize the system dynamic range on these defects. This resulted in excessive signal saturation when a strong reflector, such as the notch, was encountered. Sizing in the tandem configurations has been previously shown to be gain independent as long as the signal is strong enough to be out of the background noise, and the gain is set so there is no saturation present. The nonlinear effect of signal saturation causes dramatic oversizing to occur (i.e., an image-blooming effect is experienced). This is precisely what occurred on this notch. The final SAFT-UT sizing value of 0.20 inches was determined by performing a cursory attempt at partially compensating for this signal saturation. However, accurate TSAFT-2 sizing cannot truly occur with signal saturation present. Data collection procedures, therefore, must clearly incorporate techniques where this will be avoided.

0044

Figure 5.11 shows a photograph viewing the inside diameter of a pipe showing the N4/N5 weld in the 71.5-inch region. Dye-penetrant techniques have been employed to enhance the appearance of cracking along the area of the weld root. Notice that there is a notch and contiguous cracking which occurs on the N4 side of the weld. This area is the focus of the next line item in Table 5.4. An extracted core specimen was centered at the 71.5-inch location. Again the preliminary SAFT-UT results indicated a larger defect size than the metallurgical results found. This is due to nonlinear saturation

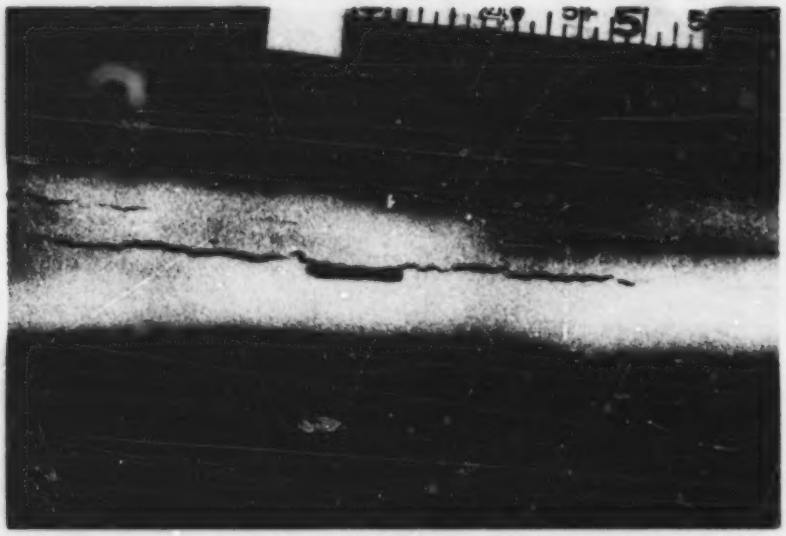

FIGURE 5.11. Photograph of Inside Diameter of N4/N5 at 71.5-inch Location

effects, previously described, from the notch reflection. When one performs SAFT-UT sizing on the crack area of this section, however, a much more realistic result is realized. The signal is not saturated in this region and accurate TSAFT-2 sizing may be performed. The final SAFT-UT value reflects this. Figure 5.12 shows the SAFT-UT pulse-echo image of the N4 weld zone from 74.0 inches to 70.25 inches in the circumferential direction. Figure 5.13 shows the corresponding TSAFT-2 image. The B-scan side-view is shown on the left-hand side and the C-scan (top-view) is shown on the right. One can see clearly the notch indication and the associated cracking contiguous to it.

Locations 15.0 and 71.5 of N5 represent areas where indications were observed in the pulse-echo images, but they appeared in the weld region or beyond the weld-center line. When this occurs, the SAFT-UT image analyst needs to recognize that the implemented configuration (shear mode) cannot reliably image defects in the weld or through the weld metal. Therefore, no call should have been made in these areas. The values in the final SAFT-UT column of Table 5.4 then have been set to zero.

BEST COPY AVAILABLE

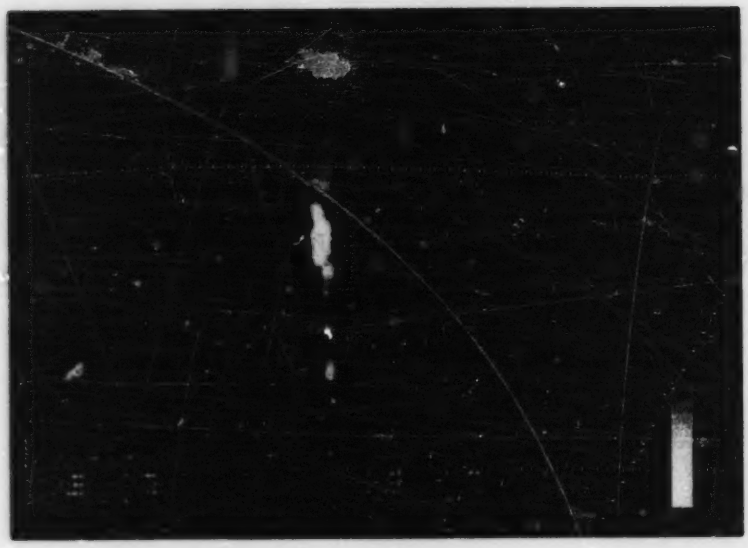

FIGURE 5.12. SAFT-UT Pulse-Echo Image of Notch and Cracking in N4 Region from 74.0 to 70.25 Inches

FIGURE 5.13. TSAFT-2 Image of Notch and Cracking in N4 Region from 74.0 to 70.25 Inches

BEST COPY AVAILABLE

At the bottom of Table 5.4 are the mean and standard deviations of the sizing results of 0.015 and 0.080, respectively, which are in good agreement with the system resolution of 2 wavelengths (see Section 4.5).

A primary goal of this exercise was to generate experience in the inspection of cracked piping and determine operating procedures to ensure maximum SAFT-UT system performance for ISI of nuclear components. The following is the procedure for data collection and image analysis of SAFT data.

5.2.1 SAFT-UT Data Collection Procedure on Piping Components:

- Normal Beam Inspection of Region of Interest. A 5-MHz normal beam scan is performed to assist in characterizing the far-surface (I.D.) contour. It assists in determining if there is an unexpected geometry condition such as severe counterbore. Also, if the weld crown has been ground smooth, this data assists in precisely locating the weld root region.

- SAFT-UT Pulse-Echo Inspection. This scan is normally performed with a 2.25-MHz, 0.25-inch-diameter transducer in the contact mode. A wedge is usually selected such that 45° shear-wave illumination is achieved. Since the primary purpose of this inspection is the detection of defects, the gain is set so that all defects of interest are detected; and if saturation of some signals occur, rescanning of them at a lower gain is necessary so that oversizing of the length does not occur.

  It is important that, as the scanning operation is occurring, the unprocessed data is viewed on the graphics design. This would allow the operator to verify the integrity of the data as it is being collected, and to flag suspected defect areas for TSAFT-2 scanning and analysis.

- TSAFT-2 Inspection. This scan is normally performed with 2.25-MHz, 0.25-inch-diameter transducers in the contact mode. Wedges are selected such that 45° shear-wave illumination is the dominant mode. This scan is selected primarily to collect vertical sizing information on suspected areas determined by the previous pulse-echo scan.

  The transducers should be arranged to optimize 3/2-Vee illumination in the region of the weld fusion line. Gains are set so that no nonlinear saturation occurs throughout the scan to be performed.

  As with the pulse-echo scan, the unprocessed data should be viewed on the graphics system as the scanning operation is occurring. This would allow the operator to verify the integrity of the data and verify that no signal saturation has occurred.

0047

5.2.2 SAFT-UT Image Analysis Procedure on Piping Components

- Normal Beam Image Analysis. The purpose of normal beam image analysis is to verify material thickness for SAFT processing of the other two configurations, and to determine if there is any unsuspected geometrical conditions at the far surface. Also, if the weld has been ground, verification of the weld-center line may be performed from this analysis.

- SAFT-UT Pulse-Echo Image Analysis. The pulse-echo image provides a very strong corner-trap indication if a surface connected reflector is present. This image is primarily used for locating the circumferential and axial defect position. It is also used to size the length of the defect.

  Since the axial position of the indication can be determined from this image, one characteristic of its validity may be observed. If the indication is located in the weld region or through the weld area, the operator should indicate that there is a low level of confidence that this indication has come from a defect.

- TSAFT-2 Image Analysis. The TSAFT-2 configuration provides a means for determining the vertical extent of a defect. SAFT processing will provide an image file that contains information for twice the pipe thickness. This gives the operator the full image, including the mirror or conjugate component. Ideally, the operator should observe a general vertical indication in the area of the defect in the B-scan side-view, with the centroid of this defect near the back-surface line on the image. If the object is significantly displaced from the back-surface line, an error in the material thickness or material velocity may have occurred. This will require reprocessing the TSAFT-2 data file with a corrected value(s). The B-scan end-view is then displayed encompassing the particular defect. The color scale must be normalized by the defect indication; and subsequently, the cursor is used to determine the full vertical extent of the defect. The 6 dB level of the normalized image has proven to be a good criterion to choose to determine a defect's vertical extent for vertical planar "crack-like" defects. To compute the final result for surface-connected defects, the value of the full vertical extent is divided by two, since the image contains both the true and mirror components.

The above data collection and analysis guidelines have been developed to assist in the data collection process to ensure data file integrity; and subsequently, to assist in the image analysis process to determine the most accurate value possible using the SAFT-UT system. The MRC data collection exercise has proven to be extremely valuable in identifying many of these procedures so that future inspections may be optimized.

0048

5.3 SAFT-UT DATA COLLECTION AND ANALYSIS ON KAPL SPECIMENS[a]

Four individual stainless steel specimens and one calibration block were received from Knolls Atomic Power Laboratory (KAPL). These specimens had an 0.25-inch to 0.5-inch overlay on the front surface and varied in thickness from 3.0 inches to 3.4 inches. A variety of unknown defects were located in them. SAFT-UT scanning was performed on these samples; both pulse-echo and tandem configurations.

The specimens were extremely narrow along one side of the scanning surface (from 1 to 2 inches). This caused severe limitations on the SAFT aperture, thus reducing lateral resolution and the signal-to-noise ratio in the resulting image. It was felt that SAFT-UT performance was favorable, especially on the parts with the thinner overlay material. However, performance relative to the deeper defects would have been enhanced if the samples were larger in the lateral dimension. No performance feedback has been received to date.

Five configurations were implemented with varying degrees of success. Initially, a series of normal-beam scans were performed on each block. This effort proved not to be fruitful and was not used in the analysis process. Forty-five degree shear wave illumination was then implemented at 2.25 MHz in the pulse-echo configuration. Also, a 45° longitudinal mode was used at 5.0 MHz. Finally, TSAFT was implemented to interrogate the area near the center of each block. Due to geometrical limitations, TSAFT-2 could not be used. The angle beam pulse-echo configurations proved to be the most useful in determining the results provided.

Some limitations in the blocks themselves, relative to SAFT-UT, should be noted. Each block was very narrow, which limited the effective SAFT aperture in the material. This reduced the advantages of SAFT processing in the deeper parts of the material. However, this geometrical attribute would not, in general, be observed in an actual field part. Also the sides of the blocks, in some cases, were very rough which may cause spurious echoes. These were accounted for in most cases, but the aperture could not be enlarged to discriminate against this effect automatically.

In general, the data was of high quality, especially in the two blocks with the thinner 0.25-inch-thick overlay. Defects in the near-surface area were detected, along with deeper flaws. Performance on the blocks with the 0.5-inch-thick overlay was degraded and fewer defects were detected.

Figure 5.14 and Figure 5.15 show beam profile plots of the transducers used in this study. These profiles were done using the calibration block to determine the effects of the cladding on the actual illumination. Figure 5.14 corresponds to the shear-wave transducer (2.25 MHz, 0.25-inch diameter, contact), and Figure 5.15 corresponds to the L-wave transducer (5.0 MHz, 0.25-inch diameter, contact). These profiles were created by placing a microprobe receiver at the back surface of the specimen and scanning the SAFT transducer

---

(a) The work on the KAPL specimens was financed by Combustion Engineering.

0049

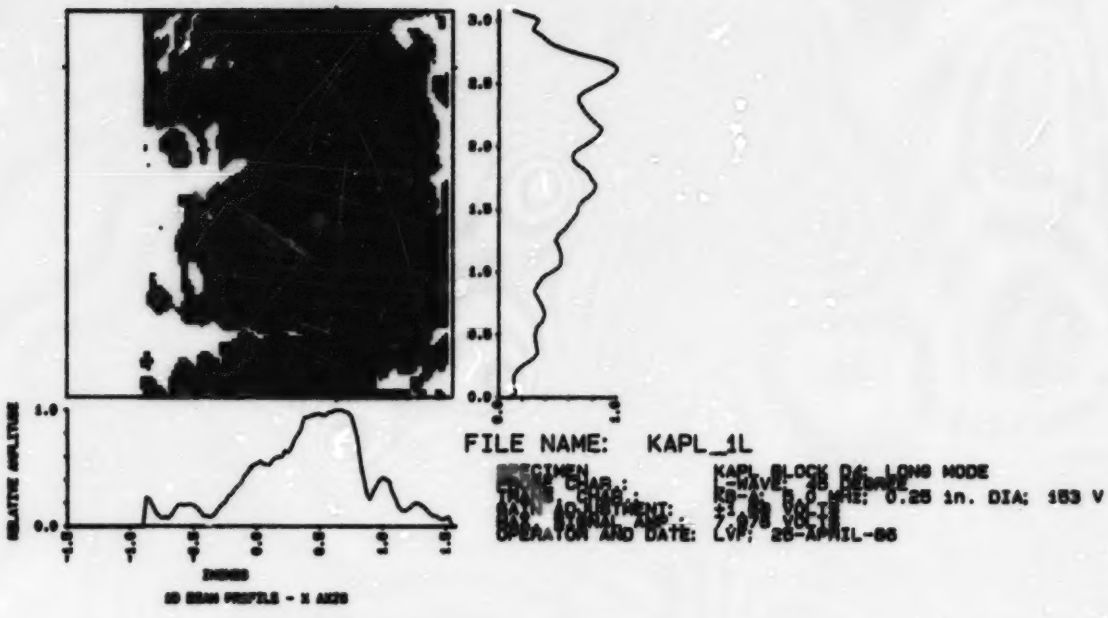

FIGURE 5.14. Transducer Beam Profile through Cladding Material. 45-degree, 5.0 MHz, L-wave

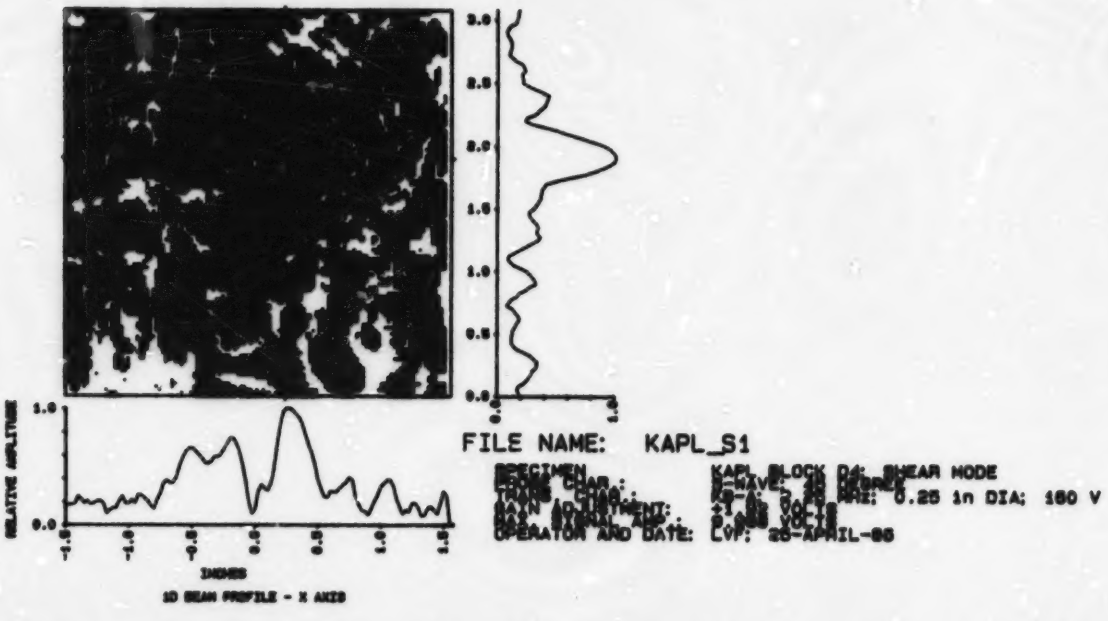

FIGURE 5.15. Transducer Beam Profile through Cladding Material. 45-degree, 2.25 MHz, S-wave

BEST COPY AVAILABLE

as the transmitter. The color scale is shown in Table 5.5. Note that the beam profiles show that there are disturbances due to the cladding, but that the general shapes are retained.

TABLE 5.5. Transducer Profile Color Scale

Color	Range, -dB
RED	0-1
ORANGE	1-2
GREEN	2-3
AQUA	3-4
BLUE	4-5
PURPLE	5-10
BROWN	10-14
BLACK	14-20
WHITE	<20

5.4 CCSS DATA COLLECTION AND ANALYSIS

Centrifugally cast stainless steel (CCSS) round robin samples were inspected by the SAFT-UT system. This material is inhomogeneous in nature due to the large grain structure formed by the manufacturing technique. There are two granular orientations that are found in this material, depending on the method of material cooling implemented during the casting process. These are termed columnar (cylindrical in geometry) and equiaxed (spherically shaped). As a result of this particular grain structure, ultrasonic inspection of piping utilizing this material historically has been difficult. Several attempts were tried for compensating for the beam skewing in this material, but assessment of these attempts is still in progress. The results on these blocks have shown that all thermal fatigue cracks in the block can be detected, but metallurgical reflectors are not able to be repeated and, thus, have lead to a high false call rate. More work is planned next fiscal year to overcome this problem.

5.5 MINI-ROUND ROBIN (MRR) IGSCC SAMPLES

Work was performed collecting data on the MRR IGSCC round robin samples. This data base contains scans of 45 quadrants on three different pipe configurations. This work, in addition to providing a significant engineering database, has also helped in establishing SAFT data collection procedures for both the pulse-echo configuration and the TSAFT configuration. Since these samples are to be destroyed, multiple scans were made to maximize the useful information that can be obtained on SAFT performance. Unfortunately, only TSAFT scans were made because the TSAFT-2 mode had not been fully developed at the time of data collection. A detailed comparison with destructive results will be made next fiscal year and provided in a topical report.

0051

6.0 CONCLUSIONS

The SAFT technology is evolving and verifying the performance predictions from its theoretical foundation. The ultrasonic principles can be used to predict the resultant images and the resolution performance. This year some significant progress was made in the adaptation of the SAFT algorithm to the TSAFT-2 or simultaneous scanned source-receiver configuration. This has resulted in improvements in the system resolution for the case of vertical planar reflectors.

The operating procedures are being defined and great care is being expended to provide a software package that is operator oriented and provides some safety checks to ensure that all the necessary information is collected to provide accurate SAFT data processing. Furthermore, the procedures are being developed to minimize errors from creeping into the data collection phase.

The permanent record by the imaging system is very valuable and useful in reviewing results as well as in the re-evaluation connected with destructive result comparisons.

The necessity for real-time operation was driven home by the extensive data bases that were generated during this reporting period. These results could have been generated in a fraction of the time that was required, if the real-time processor had been operational. Fortunately, the real-time processor unit is heading towards completion during the next fiscal year.

0052

7.0 FUTURE PLANS

The program is to be completed during the next fiscal year, and the work that must be completed includes:

- Complete the real-time processor with ten operating slave boards.
- Get the real-time processor operational for pulse-echo and thick-section files and TSAFT-2.
- Develop operating procedures for field application including piping, pressure vessels, and nozzles.
- Complete the few remaining parametric studies on system sensitivity to transducer center frequency and bandwidth.
- Develop calibration procedures for SAFT images.
- Validate the SAFT technology through field demonstrations.
- Develop full hardware specifications, software descriptions, and a technology transfer vehicle to successfully transfer the SAFT technology to the nuclear industry.
- Find a mechanism for gaining ASME Code acceptance of the SAFT technology.

0053

8.0 BIBLIOGRAPHY

Busse, L. J., H. D. Collins, and S. R. Doctor. 1984. Review and Discussion of the Development of SAFT-UT, U.S. Nuclear Regulatory Commission Report NUREG/CR-3625.

Doctor, S. R., et al. 1985. "Development and Validation of a Real-Time SAFT-UT System for Inservice Inspection of LWRs," Proceedings of the U.S. Nuclear Regulatory Commission Thirteenth Water Reactor Safety Research Information Meeting, NUREG/CP-0072, Vol 2, p. 499-519.

Doctor, S. R., L. J. Busse, S. L. Crawford, T. E. Hall, R. P. Gribble, A. J. Baldwin, and L. P. Van Houten. 1985. Development and Validation of a Real-Time SAFT-UT System for the Inspection of Light Water Reactor Components, U.S. Nuclear Regulatory Commission Report NUREG/CR-4583, Vol. 1; Semi-annual Report April-September 1984.

Ganapathy, S., B. Schmult, W. S. Wu, T. G. Dennehy, N. Moayeri, and P. Kelly. 1985. Design and Development of a Special Purpose SAFT System for Nondestructive Evaluation of Nuclear Reactor Vessels and Piping Components, U.S. Nuclear Regulatory Commission Report NUREG/CR-4365.

Krautkramer, J. and H. Krautkramer. 1977. Ultrasonic Testing of Materials, Springer-Verlag, Berlin, GDR, pp 23-45, 605-609.

0054

NRC FORM 335 (2-84) NRCM 1102, 3201, 3202

U.S. NUCLEAR REGULATORY COMMISSION

BIBLIOGRAPHIC DATA SHEET

SEE INSTRUCTIONS ON THE REVERSE

1 REPORT NUMBER (Assigned by TIDC add Vol No., if any)
NUREG/CR-4583
PNL-5822
Vol. 3

2. TITLE AND SUBTITLE
Development and Validation of a Real-Time SAFT-UT System for the Inspection of Light Water Reactor Components
Annual Report, October 1985 - September 1986

3 LEAVE BLANK

4 DATE REPORT COMPLETED
MONTH: May YEAR: 1987

5. AUTHOR(S)
SR Doctor, TE Hall, LD Reid, GA Mart

6 DATE REPORT ISSUED
MONTH: July YEAR: 1987

7. PERFORMING ORGANIZATION NAME AND MAILING ADDRESS (Include Zip Code)
Pacific Northwest Laboratory
PO Box 999
Richland, Washington 99352

8 PROJECT, TASK/WORK UNIT NUMBER

9 FIN OR GRANT NUMBER
FIN B2467

10. SPONSORING ORGANIZATION NAME AND MAILING ADDRESS (Include Zip Code)
Division of Engineering
Office of Nuclear Regulatory Research
U.S. Nuclear Regulatory Commission
Washington, DC 20555

11a TYPE OF REPORT
Technical

b PERIOD COVERED (Inclusive dates)
October 1985-September 1986

12 SUPPLEMENTARY NOTES

13. ABSTRACT (200 words or less)

The Pacific Northwest Laboratory is working to design, fabricate, and evaluate a real-time flaw detection and characterization system based on the synthetic aperture focusing technique for ultrasonic testing (SAFT-UT). The system is designed to perform inservice inspection of light-water reactor components. Included objectives of this program for the Nuclear Regulatory Commission are to develop procedures for system calibration and field operation, to validate the system through laboratory and field inspections, and to generate an engineering data base to support ASME Code acceptance of the technology. This progress report covers the programmatic work from October 1985 through September 1986.

14 DOCUMENT ANALYSIS - a KEYWORDS/DESCRIPTORS
nondestructive examination, nondestructive evaluation, nondestructive testing, inservice inspection, synthetic aperture focusing technique, signal processing, digital signal processing, ultrasonic testing

b IDENTIFIERS/OPEN-ENDED TERMS

15 AVAILABILITY STATEMENT
Unlimited

16 SECURITY CLASSIFICATION
(This page) Unclassified
(This report) Unclassified

17 NUMBER OF PAGES

18 PRICE

☆ U.S. GOVERNMENT PRINTING OFFICE:1987-187-008

0055

UNITED STATES
NUCLEAR REGULATORY COMMISSION
WASHINGTON, D.C. 20555

OFFICIAL BUSINESS
PENALTY FOR PRIVATE USE, $300

SPECIAL FOURTH-CLASS RATE
POSTAGE & FEES PAID
USNRC
WASH. D.C.
PERMIT No. G-67

FOR THE INSPECTION OF LIGHT WATER REACTOR COMPONENTS

056